EUROPEAN ORGANIZATION FOR NUCLEAR RESEARCH

CERN SL/95-25 (AP)

Simulation of Single-Bunch Collective Effects in LEP by Linear Expansion of the Distribution Moments

G. Sabbi *

Abstract

A new method for modelling wakefield effects in multi-particle tracking programs is presented. This method, which is based on an expansion of the particle distribution and its dipole moment into a basis of linear interpolating functions, is first described in some detail, and compared with previous approaches to wakefield representation. Using a refined impedance model, the reference (basis function) wakes in the LEP structures are then computed. The problems concerning the definition of a suitable accelerator model in the simulation program are discussed; the stability of the results with respect to the choice of the number of macroparticles, of the length of the basis function, and of the machine model is investigated, and the performance is compared with that obtained by expanding the distribution into a basis of Hermite polynomials. Finally, a few applications to the study of collective effects in LEP are presented, aiming at both assessing the reliability of the simulation results and at better understanding observations made during machine experiments.

Geneva, Switzerland

May 9, 1995

* CERN Doctoral Student Programme

1 Introduction

Numerical simulation is an important tool in the study of collective effects, which are responsible for severe limitations of the bunch current in electron storage rings. Here a new technique for the calculation of the wake contribution to the beam dynamics is presented, in which the particle distribution and its first moment are expanded into a basis of linear (triangular-shaped) interpolating functions. This approach, compared with other techniques computing the wake as sums of either super-particle or Hermite polynomial contributions, permits improving the description of the distribution, in particular near the stability threshold, where it is usually quite non-Gaussian. At the same time, both the computation time and the memory requirements are decreased by large factors, allowing for the use of more realistic machine representations.

The TRISIM program [1], which simulates the 2D (longitudinal-vertical) motion of N superparticles in a circular machine, is based on the new distribution representation method, while relying on a more classical formalism as far as the description of the single particle dynamics is concerned. The program has been successfully tested on the experimental data of LEP: with a refined impedance model, in which contributions from resonant cavities (both copper and superconducting), separators, tapers and bellows of different kind are taken into account, a quite good agreement with measurements was obtained, in particular for the threshold of transverse mode coupling, which is limiting the single bunch current most severely. The code has also been applied to the study of feedback systems, and to the study of machines other than LEP.

This report presents a description of the distribution function representation technique, the impedance model, and some of the results which have been obtained.

2 The simulation program TRISIM

2.1 Single particle dynamics

The geometry of the machine is modelled by a ring divided into a given number of sectors, each one composed by a point-like element followed by an arc section in which the motion is assumed linear. A set of multi-charged particles ("macroparticles", "superparticles") represents the charge distribution in the bunch, and, starting from suitable initial conditions, their dynamical evolution in a 2D (longitudinal-vertical) plane is simulated. The motion of the superparticles is described in terms of energy deviation ϵ and time delay t with respect to the synchronous particle, plus the vertical position z and its slope z'.

As far as the description of single particle dynamics is concerned, the new program TRISIM uses essentially the same formalism as HERSIM2 [2], which was derived from its predecessors HERSIM [3] and SIMTRAC [4]; only minor modifications in the equations of motion have been included (as suggested in [5]), and a few element classes have been added. However, since the related informations are spread in many different publications, the equations of motion which are presently used in the program will be reported here for reference purposes.

The point-like elements represent structures for which the length is sufficiently short that it can be neglected. This means that the betatron phase does not change very much in traversing the structure, and that the optical functions of the storage ring are approximately constant over its length. The interaction between the beam and the element can then be represented as a kick: the coordinates t and z of each particle are unaffected by passing through the structure, and only the moments ϵ and z' can be modified.

The element classes which are taken into account are: RF cavity, impedance, sextupole, pick-up, kicker. The equations for the passage through these elements are:

- RF cavity:

$$\begin{aligned} E_i &= \epsilon_i + eV_i^{RF}\sin(\Phi_i^s + \omega_i^{RF} t_i) + \delta\epsilon_i \\ Z_i' &= z_i' + \delta z_i' \end{aligned}$$

  where

V_i^{RF} ω_i^{RF}	are the amplitude and the angular frequency of the RF wave
Φ_i^s	is the phase of the synchronous particle with respect to the RF wave
$\delta\epsilon_i$ $\delta z_i'$	are the longitudinal and transverse kicks due to the wakefield

- Impedance:

$$\begin{aligned} E_i &= \epsilon_i + \delta\epsilon_i \\ Z_i' &= z_i' + \delta z_i' \end{aligned}$$

  where $\delta\epsilon_i$ e $\delta z_i'$ represent the longitudinal and transverse kicks due to the wakefield.

- Sextupole:

$$\begin{aligned} E_i &= \epsilon_i \\ Z_i' &= z_i' + k_i' d_i \epsilon_i z_i \end{aligned}$$

  where

k_i'	is the sextupole strength in units of m^{-2}
d_i	is the horizontal dispersion

  The intensity of the sextupolar field is determined according to

$$k' = eLG'/p$$

  where e is the unit of charge, L is the length of the sextupole, G' is the derivative of the sextupole field gradient and p is the average momentum of the beam particles.

- Kicker:

$$\begin{aligned} E_i &= \epsilon_i \\ Z_i' &= z_i' + \theta \end{aligned}$$

  where θ is the deflection angle, which is assumed to be independent of the position and energy deviation of the particle.

The equations of motion for the arc section are:

$$
\begin{aligned}
z_{i+1} &= \mathcal{M}_{11}(E_i) z_i + \mathcal{M}_{12}(E_i) Z'_i + \sqrt{\frac{2\mathcal{E}_z \bar{\beta} T_0}{\tau_z}} R_i^1 \\
z'_{i+1} &= \mathcal{M}_{21}(E_i) z_i + \mathcal{M}_{22}(E_i) Z'_i + \sqrt{\frac{2\mathcal{E}_z}{\bar{\beta} T_0 \tau_z}} R_i^2 \\
\epsilon_{i+1} &= E_i - u_i + 2\sigma_\epsilon^o \sqrt{\frac{T_0}{\tau_\epsilon}} R_i^3 \\
t_{i+1} &= t_i + \alpha T_i \left[\frac{E_i + E_r}{E_r} \frac{\ln(1+Q_i)}{Q_i} - 1 \right]
\end{aligned}
$$

where the following definitions have been used:

$$
\begin{aligned}
\mathcal{M}_{11}(E_i) &= \exp\left(-\frac{T_i}{\tau_z}\right) \sqrt{\frac{\beta_{i+1}}{\beta_i}} \cos(\Psi_i(E_i)) \\
\mathcal{M}_{12}(E_i) &= \sqrt{\beta_{i+1}\beta_i} \sin(\Psi_i(E_i)) \\
\mathcal{M}_{21}(E_i) &= \exp\left(-\frac{T_i}{\tau_z}\right) \frac{1}{\sqrt{\beta_{i+1}\beta_i}} \sin(\Psi_i(E_i)) \\
\mathcal{M}_{22}(E_i) &= \sqrt{\frac{\beta_i}{\beta_{i+1}}} \cos(\Psi_i(E_i)) \\
u_i &= (E_r + E_i) \frac{Q_i}{1+Q_i} \\
Q_i &= U_i \frac{E_r + E_i}{E_r^2} \\
\Psi_i(E_i) &= \Phi_i^o \left[1 + \left(\xi_i - \frac{\eta}{E_r} \right) \left(E_i - \frac{1}{2} u_i \right) \right]
\end{aligned}
$$

and with the following notations:

T_0 Revolution time of the reference particle.

T_i Transit time of the reference particle through the i-th sector.

Φ_i^0 Betatron phase advance of the reference particle in the i-th sector.

U_i Synchrotron radiation energy loss in the i-th sector.

E_r Nominal energy.

σ_ϵ^o RMS energy spread.

τ_ϵ Energy damping time.

τ_z Vertical damping time.

β_i β function at the i-th (point-like) element.

$\bar{\beta}$ Average β in the ring: $\bar{\beta} = R/Q_v$, where R is the average radius and Q_v is the vertical tune.

$\mathcal{E}_z$ Vertical emittance: $\sigma_z(s) = \sqrt{\beta(s)\mathcal{E}_z}$.

ξ_i Chromaticity in the i-th sector: $\xi = (\delta Q/Q)/(\delta p/p) = Q'/Q$.

α Momentum compaction factor: $\alpha = (\delta C/C)/(\delta p/p)$. C is the accelerator circumference.

η Momentum slip factor: $\eta = \alpha - 1/\gamma^2$.

$R_i^{1,2,3}$ Random numbers with normal distribution.

2.2 Wakefield representation

The wakefield representation technique is based on the assumption that the structures generating the wakes are axially symmetric. In these conditions, it is convenient to adopt a cylindrical coordinate system (r, θ, s) and to express a general (3D) charge distribution as sum of multipole moments I_m, i.e. distributions which have a harmonic dependence on the azimuth. The multipole moments form a complete set. In an axially symmetric structure, each element of the expansion will generate wakefields which again have a harmonic dependence on the azimuth, of the same order as the generating multipole moment ([6], §2.1).

If the wake comes from structures which are of a size comparable to the pipe radius b, the longitudinal wake force scales as $(a/b)^{2m}$, and the transverse wake force as $(a/b)^{2m-1}$, where a is the transverse beam size ([6], §2.2). Since usually $b \gg a$, the $m = 0$ component dominates the longitudinal wake effects, and the $m = 1$ component dominates the transverse wake effects, while the effect of higher moments can generally be neglected.

The wake force $\vec{F}$ experienced by a (point-like) trailing test particle can be a complicated function of position and time. However, at high energies, the trajectories of the beam and the test charge are not perturbed much as they travel through the structure, and it is convenient to introduce the integrated impulses:

$$\vec{U} \equiv \int_0^L \vec{F}\, ds$$

In the simple case of a point-like generating charge, neglecting the contributions from higher order multipole moments, and projecting on a cartesian reference system (x, y, s), the following expressions for the integrated impulses can be derived ([6], §2.2):

$$\vec{U}_{\parallel}(\zeta) = -\mathrm{eq}W_0'(\zeta)\hat{s} \quad (1)$$
$$\vec{U}_{\perp}(\zeta) = -\mathrm{eq}W_1(\zeta)(a_x\hat{x} + a_y\hat{y}) \quad (2)$$

where W_m is the response of the structure to the the m-th multipole moment I_m of a unit point-like source charge, and is called the wake function. W_m is a function of ζ, the distance between the generating and the test particle; q is the charge of the source particle, with coordinates (a_x, a_y) in the transverse plane; e is the charge of the test particle.

Equation (2) shows that the vertical and horizontal contributions to the transverse impulse are decoupled in this approximation, so that the particle motion in the two directions can be studied independently.

A first solution for incorporating wakefield effects into a computer model consists in the direct application of the equations (1), (2) to the macroparticle distribution [4]. However, this approach encounters serious difficulties. The wake functions $W_m(\zeta)$ of a point charge (δ-function wake) are in fact impossible to obtain analytically except for a very few, over-simplified structures. Severe difficulties also emerge when one tries to compute a wake function numerically, because of a singularity in the time domain and the infinite number of resonances required in the frequency domain. Although several approximations in the time domain have been proposed [8, 9, 10], it is not clear that these approximations can give satisfactory results for all cases. Apart from these problems, the direct use of the macroparticle set in the calculation of the wakefield kicks leads to an amplification of the effect of the statistical fluctuations in the macroparticle distribution, with respect to the physical reality. This is due to the use of a limited set of macroparticles in the simulation (one macroparticle represents about 10^8 elementary charges), together with the discontinuity of the longitudinal wake function at ζ=0, and, in the case of LEP, to the presence of significant high frequency components in the transverse impedance. As a consequence, a close encounter between two macroparticles can lead to rather different results, depending on small differences in the macroparticle positions. This effect is responsible for the observed strong dependence of the results on the number of macroparticles employed [11]. Increasing the number of macroparticles (N) until stability is reached would be a costly solution in terms of CPU time; however, since the dependence of the results on N has been shown to follow, to a good accuracy, a rather simple quadratic law [11], this problem can be overcome by performing two runs with different N, and computing the asymptotic values.

In view of the difficulties encountered when dealing directly with point charges, it is convenient to construct an averaged (continuous) density function ρ_c starting from the macroparticle distribution. If $(x^{(n)}, y^{(n)}, s^{(n)})$ are the coordinates of the macroparticles at the impedance location, the discrete charge distribution can be written as

$$\rho_d(x, y, s) = \mathrm{q} \sum_{n=1}^{N} \delta(x - x^{(n)})\delta(y - y^{(n)})\delta(s - s^{(n)})$$

For charge conservation, the density function ρ_c will have to satisfy the property:

$$\int_\Omega \rho_c(x, y, s)\, dxdyds \simeq \int_\Omega \rho_d(x, y, s)\, dxdyds \tag{3}$$

in each integration domain Ω containing a sufficiently high number of macroparticles.

From equations (1), (2) it is rather straigthforward to derive an expression for the wakefield kicks experienced by a bunch of spatial charge distribution ρ_c:

$$\vec{U}_{\parallel}(s') = -e\hat{s} \int \lambda(s) W_0'(s' - s)\, ds \tag{4}$$

$$\begin{aligned} \vec{U}_{\perp}(s') &= -e\hat{x} \int \lambda(s)\bar{x}(s)\, W_1(s' - s)\, ds - \\ &\quad -e\hat{y} \int \lambda(s)\bar{y}(s)\, W_1(s' - s)\, ds \end{aligned} \tag{5}$$

where s is spanning the generating charge distribution, s' is the position of the test particle, and the following definitions have been used:

$$\begin{aligned}
\lambda(s) &\equiv \int \rho_c(x,y,s)\, dxdy \\
\bar{x}(s) &\equiv \frac{1}{\lambda(s)} \int x\, \rho_c(x,y,s)\, dxdy \\
\bar{y}(s) &\equiv \frac{1}{\lambda(s)} \int y\, \rho_c(x,y,s)\, dxdy
\end{aligned}$$

The details of the derivation can be found in [7]. In the case of a source distribution of finite spatial extent, the integrated impulse experienced by an unit test charge $\vec{V} = \vec{U}/e$ is called the wake potential. Equations (4), (5) show that the wake potentials due to the longitudinal $m = 0$ and the transverse $m = 1$ multipolar components of the charge distribution can be computed from the quantities:

$$\lambda(s) \qquad ; \qquad \lambda(s)\bar{x}(s) \qquad ; \qquad \lambda(s)\bar{y}(s) \tag{6}$$

In practice, it is usually more convenient to derive the distribution moments (6) directly from the discrete distribution function ρ_d, instead of constructing the continuous distribution function ρ_c explicitly, and to express them as sums over a suitable set of basis functions with finite length. For example, the longitudinal charge density $\lambda(s)$ will be written:

$$\lambda(s) = \sum_{k=1}^{M} \alpha_k\, \lambda_k(s)$$

and the longitudinal wake potential will be expressed as:

$$\vec{V}_{\parallel}(s') = \sum_{k=1}^{M} \alpha_k\, \vec{v}_{\parallel}^{(k)}(s')$$

with

$$\vec{v}_{\parallel}^{(k)}(s') = \int \lambda_k(s) W_0'(s'-s)\, ds$$

and similarly for $\vec{V}_{\perp}^{(k)}(s')$. It is worth noting that the orthogonality of the elements of the basis is not required in this process. The elementary quantities for the wake potential calculation have now become the $\vec{v}_{\parallel}^{(k)}(s')$, $\vec{v}_{\perp}^{(k)}(s')$, which can be obtained by numerical solution of Maxwell equations, without explicitly refererring to the wake functions[1] $W_m(\zeta)$. The problem is then shifted to the choice of the basis functions, the quality of which has to be evaluated against the following criteria:

- Accuracy in the description of a general distribution, for a fixed, finite number of basis functions.

[1] However, if the wake function is known to a sufficient accuracy, it can be used as a Green function to compute the reference wake potentials, see section 4.

- Time needed to compute the coefficients of the expansion.
- Accuracy in the calculation of the wake potential of the basis distributions by an electromagnetic analysis code, for given computational resources.
- Number of independent calculations needed to obtain the basis function wake potentials.

An example of application of this approach is represented by the simulation program HERSIM [3], in which the distribution moments are expressed as sums of low order Hermite polynomials, normalized to the rms bunch length σ at the location of the impedance. In this approximation, the longitudinal charge density will be written:

$$\lambda(s) \approx \exp\left(-\frac{(s-\bar{s})^2}{2\sigma^2}\right)\sum_{l=0}^{L}\alpha_l \mathrm{He}_l\left(\frac{s-\bar{s}}{\sigma}\right)$$

In a typical HERSIM run the series is truncated at the order 6, and 15 sets of wakes, corresponding to basis functions of different order and azimuthal mode number (m=0 and m=1), are precalculated and stored in 2-D look-up tables for suitable ranges of σ and s.

Since the equilibrium bunch distribution at low currents is a Gaussian, a set of Hermite polynomials, which are essentially derivatives of the Gaussian, seems particularly appropriate to represent it, and should give a good approximation already at low orders.

On top of this, it was shown [12] that the wake potential due to a Gaussian distribution can be calculated from the wake of a Gaussian with a smaller standard deviation, and that the wake potential of an Hermitian distribution of order n can be obtained, with n derivations, starting from the wake potential of the Gaussian [13]. The wake potentials for the whole set of basis functions can then be all generated starting from just one wake potential calculation, relative to a Gaussian distribution of the smallest standard deviation[2].

The advantages of the Hermite polynomial representation, as compared to the δ-function wake approach, are the good stability of the result with respect to the number of macroparticles employed, and the possibility of including impedances with high characteristic frequencies in the model. On the other hand, the choice of the Hermite polynomials as basis functions, which is the key element of this technique, is also responsible for its main limitations. This basis is indeed well suited for representing a pseudo-Gaussian distribution at low current; but at higher currents, and particularly in the proximity of the stability threshold (i.e. in the situations which are more interesting to study) the distribution tends to depart significantly from the equilibrium one, and the number of terms which would be necessary to represent it accurately with the Hermite polynomial basis increases. Since the series is truncated at the sixth order, the quality of the representation degrades as the current increases. This problem is reflected, for example, in a greater difficulty in chosing the optimal σ for the representation: this choice is then based on a set of criteria mainly derived from experience, relatively complicated to implement, and with results which are not always satisfactory. A second drawback is related to the set-up and handling of the wake tables (15 tables, each one a 2-D array 25x640), and to the computer time spent in building the wake potential for the chosen bunch length by interpolating between the closest tables.

[2]It should be noted, however, that in order to compute the wake potential of a short bunch a fine mesh is necessary, and in order to use this wake to compute the wake of longer bunches one needs to extend the calculation to a (comparatively) rather large distance behind the short bunch. In practice, it may be more efficient to perform independent calculations using different mesh sizes. It is also worth noting that, if the wake potential of the Gaussian distribution is obtained by numerical solution of Maxwell equations, the use of numerical derivations to compute the wakes of the higher order Hermite polynomials leads to a rapid loss of accuracy. Better results can be obtained if the wake is computed analytically for a broad band resonator model [14].

In what follows, an alternative technique for the wakefield representation is presented, based on the approximation of the longitudinal charge density of the distribution, $\lambda(s)$, and its dipole moment, $d(s)$, by a sum of triangular shaped basis functions of constant width and variable height. In the case of a 2-D (s, z) representation of the dynamics[3], the wakefield representation proceeds as follows:

- A longitudinal interval $[s_0, s_M]$ is defined, whose extremes correspond to the single-particle stability limits, outside which the particle is considered to be lost.
- The interval is divided into M uniform segments, the length of which is given by

$$\Delta = (s_M - s_0)/M$$

  The quantity Δ corresponds to the set Ω appearing in the equation (3), that is an integration domain over which a continuous density function can be defined. An increase of Δ will correpond to a stronger filtering of the high frequency components of the distribution: the length Δ should be chosen in such a way as to filter out those oscillations which are due to the limited number of macroparticles employed, retaining at the same time the physical information about the charge distribution. On the basis of the experience, the choice of Δ is not extremely critical for the stability of the simulation results: if σ is the longitudinal rms of the distribution, Δ can be safely chosen in the interval

$$\Delta \in \left[\frac{\sigma}{5}, \frac{\sigma}{2}\right]$$

  where the upper limit is set by the accuracy requirements in the wakefield representation, while the lower limit is set both by the length of the computed reference wake potential and by the number of macroparticles to be employed in the simulation. In fact, for a initially Gaussian distribution extending over a longitudinal interval of length 10σ, the minimum number of macroparticles which are needed to have a statistically significant resolution of the order of Δ can be estimated as:

$$N \approx F \left(\frac{10\sigma}{\Delta}\right)^2 \tag{7}$$

  where F can vary in the interval $[1, 2]$ depending on the higher current bunch dynamics: for example, a simulation of the bunch lengthening phenomenon, in particular in the presence of turbulence, tends to require a larger N, because higher order modes are involved in the dynamics.
- For each of the nodes $s_k = s_0 + k\Delta$ in the interval $[s_0, s_M]$, excluding the two extremes where the condition $\rho = 0$ is imposed, a linear interpolating function f_k, centered on the node itself, and extending over the segment $[s_{k-1}, s_{k+1}]$, is introduced:

$$f_k(s) = \begin{cases} 1 - \mid s - s_k \mid /\Delta & s \in [s_{k-1}, s_{k+1}] \\ 0 & s \notin [s_{k-1}, s_{k+1}] \end{cases} \tag{8}$$

[3]The longitudinal coordinate s is relative to the position of the synchronous particle.

- The distribution moments $\lambda(s)$ and $d(s)$ are defined as weighted sums of the functions f_k:

$$\lambda(s) = \sum_{k=1}^{M-1} \lambda_k \, f_k(s) \tag{9}$$

$$d(s) = \sum_{k=1}^{M-1} d_k \, f_k(s) \tag{10}$$

A graphical illustration of this representation technique is given in figure 1 (M=6). In practice, values of M between 20 and 50 are used.

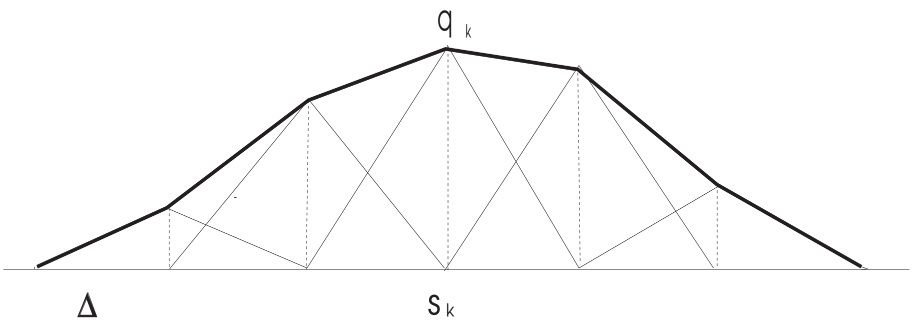

Figure 1: Distribution representation as sums of linear interpolating functions (M=6).

- The coefficients λ_k e d_k are obtained as sums of contributions $\delta\lambda_k^{(n)}$, $\delta d_k^{(n)}$ from the macroparticles, of coordinates $(z^{(n)}, s^{(n)})$, composing the bunch:

$$\lambda_k = \sum_{n=1}^{N} \delta\lambda_k^{(n)} \qquad ; \qquad d_k = \sum_{n=1}^{N} \delta d_k^{(n)}$$

- The contribution of each macroparticle to the coefficients λ_k of the longitudinal charge density is calculated according to the formula:

$$\delta\lambda_k^{(n)} = \begin{cases} (1-|s^{(n)} - s_k|/\Delta)\, \mathrm{q}/\Delta & s^{(n)} \in [s_{k-1}, s_{k+1}] \\ 0 & s^{(n)} \notin [s_{k-1}, s_{k+1}] \end{cases} \tag{11}$$

The meaning of the expression (11) is the following: the contribution to the charge density of a macroparticle of longitudinal coordinate sitting in the interval $[s_{k-1}, s_k]$ is shared between the interpolating functions centered at the two extremes of this segment, in a way proportional to the relative distance of the macroparticles from these two points:

$$\begin{aligned} \delta Q_{k-1}^{(n)} &= \Delta\, \delta\lambda_{k-1}^{(n)} &= \mathrm{q}\, [1 - (s^{(n)} - s_{k-1})/\Delta] \\ \delta Q_k^{(n)} &= \Delta\, \delta\lambda_k^{(n)} &= \mathrm{q}\, [1 - (s_k - s^{(n)})/\Delta] \end{aligned}$$

and the sum of the two area contributions is q, the charge of the macroparticle.

- The contribution of each macroparticle to the coefficients d_k of the dipole moment is calculated according to the formula:

$$\delta d_k^{(n)} = z^{(n)} \delta\lambda_k^{(n)}$$

so that the desired area increment to the dipole moment is obtained, $\delta D^{(n)} = z^{(n)}\, \mathrm{q}$.

- The longitudinal ($m = 0$) and transverse ($m = 1$) wake potentials in a given axially symmetric structure are finally obtained as:

$$V_{\|}(s) = \sum_{k=1}^{M-1} \lambda_k v_{\|}(s - s_k) \quad (12)$$

$$V_{\perp}(s) = \sum_{k=1}^{M-1} d_k v_{\perp}(s - s_k) \quad (13)$$

where $v_{\|}$ and $v_{\perp}$ are the wake potentials due to a "hollow beam" (an infinitesimally thin ring of charge with unit radius), carrying a pure mth multipole moment, with a longitudinal density given by $f_k(s)$. The details of this calculation, which is usually performed by means of an electromagnetic mesh code, are described in section 4. In practice, the reference wakes will be tabulated at a sequence of discrete positions, and the resulting wake will also be given at discrete intervals, the length of which is tipically chosen as $\Delta/3$. The wake potential at each particle position is then computed by interpolation between the closest points.

The key element in this wakefield representation technique is the use of linear functions: first, it allows a full exploitation of the linearity of Maxwell equations in the calculation of the wake potential; second, the resulting procedure is very well suited to the implementation on a digital computer. The use of linear functions results in the following advantages:

- A single reference wake potential for each direction (longitudinal, transverse) is sufficient to compute the wake of a general distribution, the length of which can vary over a relatively wide range.
- The wake potential calculation is fast and easy to implement; no special case has to be taken into account.
- The quality of the approximation does not depend on the bunch having any pre-determined shape.
- A definite positive representation of the charge density is automatically ensured.
- The wake potential of a basis function of length Δ can be used[4] to compute the wake potential of a basis function the length of which is a multiple of Δ.

For what concerns the disadvantages of this technique, the main one is related to the presence of discontinuities in the first derivative of the basis function, which makes the numerical calculation of its wake more difficult with respect to that of a smooth distribution of the same length: this happens because the sharp distribution can excite, in the structure, modes of higher order with respect to those which would be excited by the smooth one. The various aspects of the calculation of the basis function wake potential are discussed in detail in section 4.

One should also note that the discontinuities of the first derivative in the piecewise linear approximation of the distribution moments do not correspond to the physical reality, and that

[4] As it was already mentioned, however, the use of the long-range wake of a short bunch to compute the wake of a longer bunch is not very efficient from the point of view of the computational resources. For what concerns an hypothetical "deconvolution" of the wake a longer bunch, in order to obtain the wake of a shorter one, it would lead to a solution in which the high frequency components have been filtered out, and to an amplification of the numerical errors [13].

the distribution representation depends, to some extent, on the choice of the s_k positions in which the linear interpolating functions are centered. However, the origin of these problems is not in the distribution representation method, but in the use of a limited set of macroparticles. In fact, the only criterium for judging the quality of the distribution representation is given by equation (3); if an infinite number of macroparticles is used, any small integration domain Ω can be chosen, and all the representations must converge to the same function. For a limited number of macroparticles, however, for stability reasons[5] only larger integration volumes can be chosen, and there is no "best" representation among those which satisfy the integral criterium.

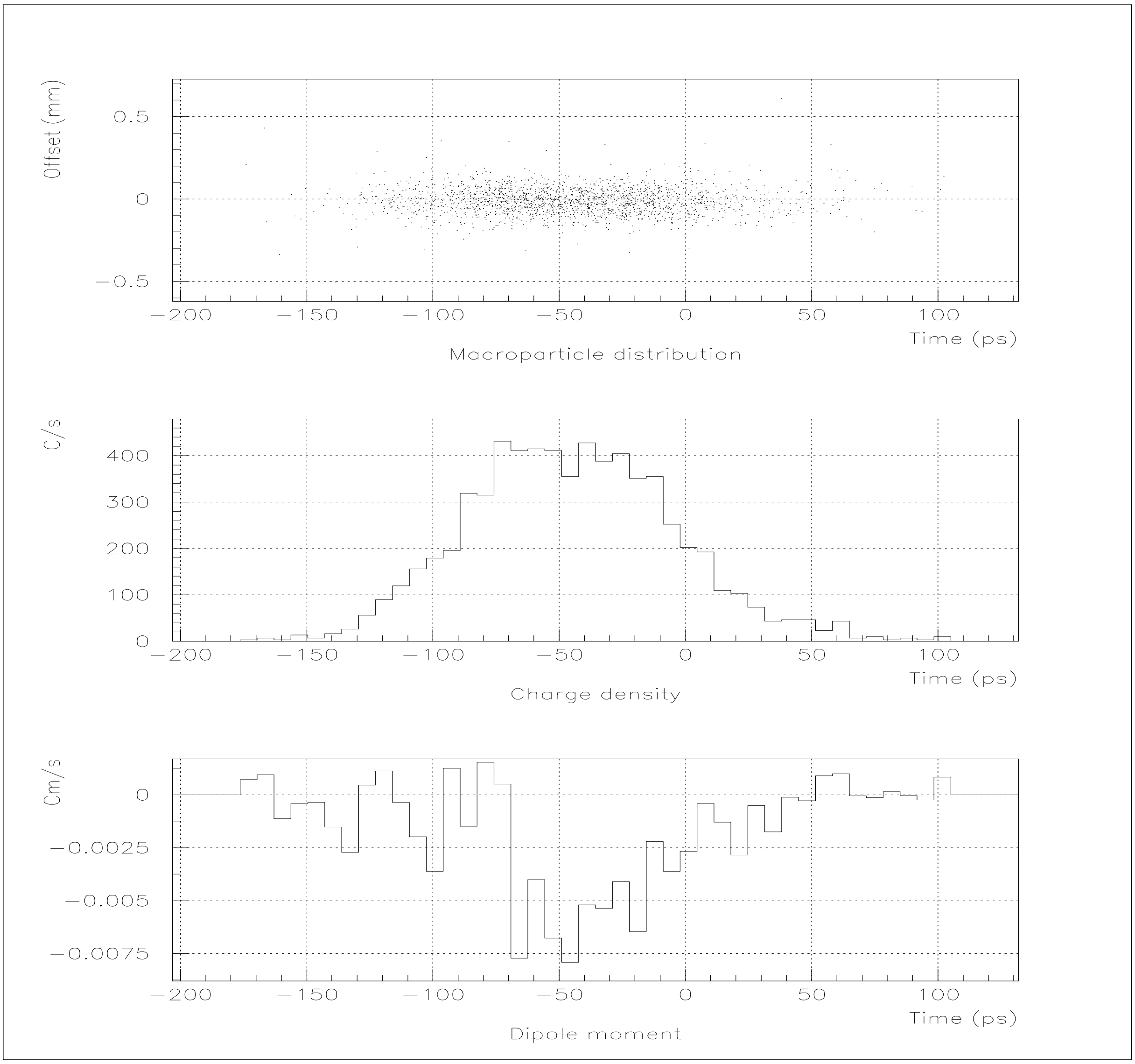

Figure 2: Example of a macroparticle configuration during the tracking.

To further illustrate the wake potential calculation method in terms of linear interpolating functions, an example is given in what follows. Here the method is applied to the macroparticle configuration which is reported in figure 2; two histograms are also reported, the first relative to the charge density, the second relative to the dipole moment of the distribution.

[5]The integral at the left hand side of equation (3) should be a smooth function of Ω.

It should be noted that in the first plot the vertical axis scale is much enlarged with respect to the horizontal one (≈ 20 times), so that the cross section is in reality much thinner than it appears in the picture. The number of macroparticles which have been used is 2000, and the distribution is approximately Gaussian, with an rms length $\sigma_t \approx 40$ ps. The macroparticles extend over a longitudinal interval of about 300 ps (9cm), corresponding to $7.5\sigma_t$. The oscillations which appear in the histograms, in particular in the one relative to the dipole moment, are partly due to the coherent beam oscillations, and partly to the statistical fluctuations in the "discrete" macroparticle distribution ρ_D.

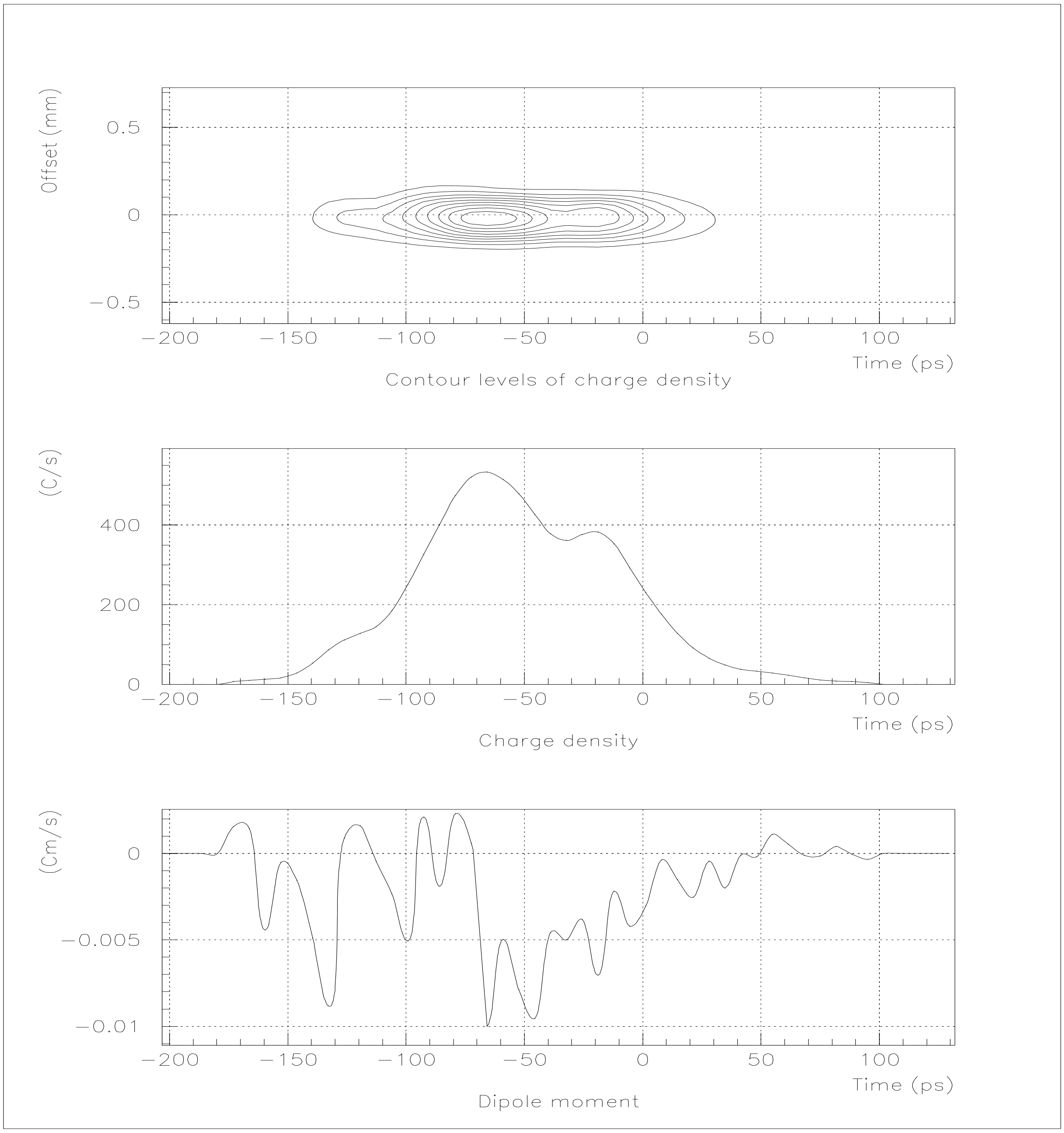

Figure 3: Example of a continuous (2-D) distribution function, and of its moments.

Figure 3 shows how, starting from the macroparticle configuration of figure 2, it is possible to construct a continuous distribution function ρ_C, represented by contour levels in the first plot, and subsequently projected on the longitudinal axis in order to obtain the zero-order (charge density) and the first-order (dipole) moments. The function ρ_C has been obtained with the B-splines method [32], and depends to some extent on the chosen parameters, namely the number of nodes and the order of the splines. The function ρ_C is not used for the wake potential calculation in the simulation, both because its calculation is rather long and because it cannot be directly expressed as sums of basis functions; however, the countinuous distribution function is very useful in the analysis of the simulation results: the countour level representation helps recognize the structures due to coherent oscillations, while the continuous representation of the distribution moments is prefered to the histograms of figure 2, because it is less sensitive to the choice of the size of the bins.

Figures 5 and 4 show how the distribution of figure 2 is represented as sums of linear interpolating functions, and how the longitudinal and transverse wake potentials are computed.

The histograms of the distribution moments, which are not used for the calculation, are reported, for comparison, in the first plot of each figure.

The second plot reports the representation of the distribution moments as sums of linear interpolating functions with half-length Δ=20 ps, as expressed by equations (9) and (10). It shows how this choice of Δ allows to correcly represent the relevant structures, while the statistical fluctuations of the histograms are filtered out. In this example, 18 basis functions are used to represent the distribution.

In the third plot of each figure the longitudinal and transverse wake potentials of the basis distribution, that is the functions which were previously indicated as $v_T(s)$ and $v_L(s)$, are reported. In this case, $v_T(s)$ and $v_L(s)$ are effective wakes corresponding to the total impedance which is seen by a bunch during a complete turn around the LEP accelerator. They are obtained as weighted sums of the elementary wakes corresponding to each structure, taking into account the total number of structures in the machine, and the average values of the β function at each impedance class. The various aspects of the calculation of the reference wake potentials are discussed in section 4, while the possibility of combining the wakes of different structures into a single "effective" wake is discussed in section 5.

By linearly combining the reference wakes, according to equations (12) e (13), the longitudinal and transverse wake potentials of the distribution are finally obtained, as reported in the fourth plot of, respectively, Fig. 5 (longitudinal) and Fig. 4 (transverse).

The so obtained potentials are then used to compute the wakefield effects on the particles of the distribution: for a bunch charge of about 45 nC, corresponding to a bunch current of 0.5 mA, the one-turn kick received by each particle due to collective effects is, in LEP, of the order of 10 MeV in the longitudinal plane, and 10 keV in the vertical plane, to be compared with a particle energy of 20 GeV at injection.

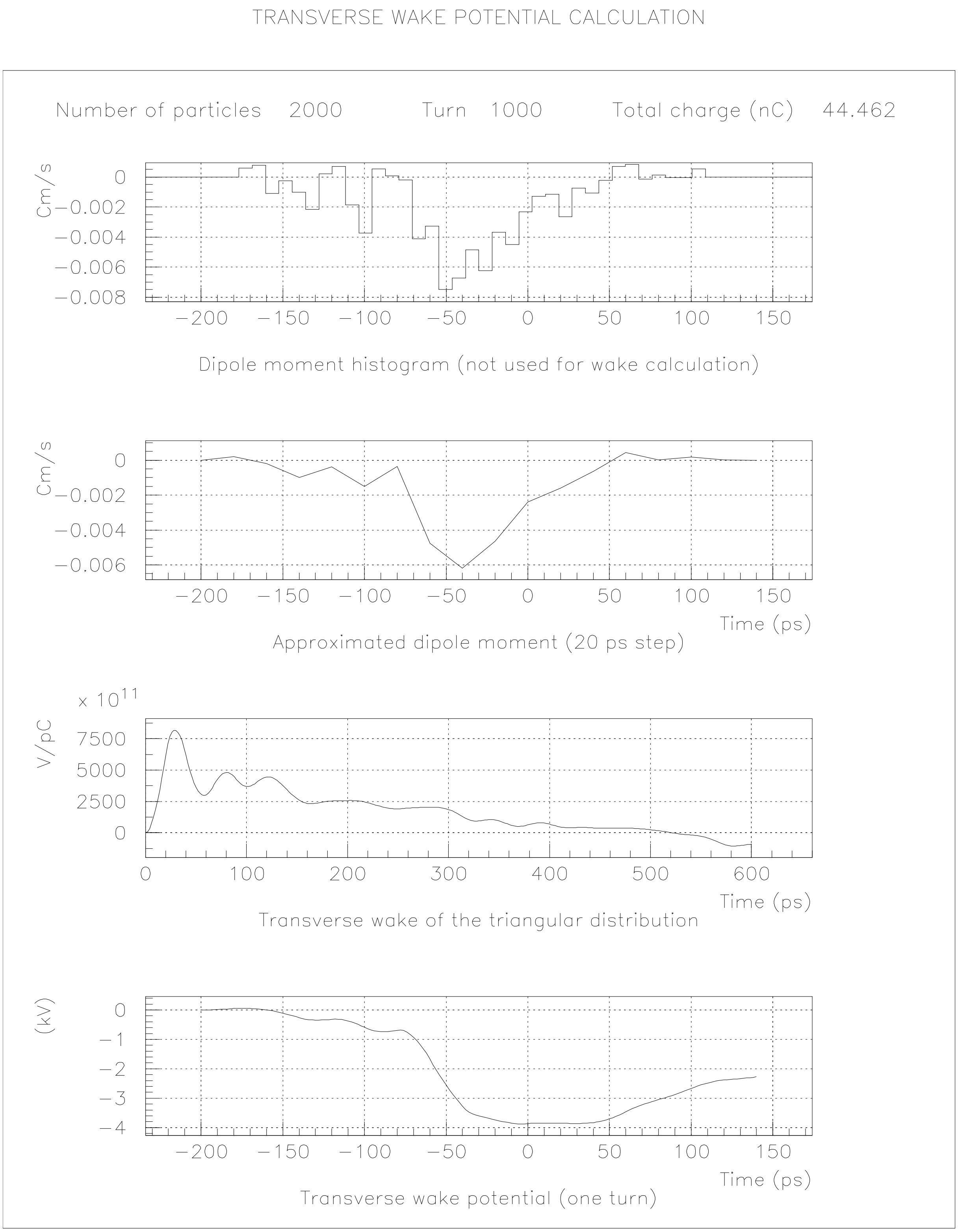

Figure 4: Calculation of the transverse wake potential (Δ=20 ps).

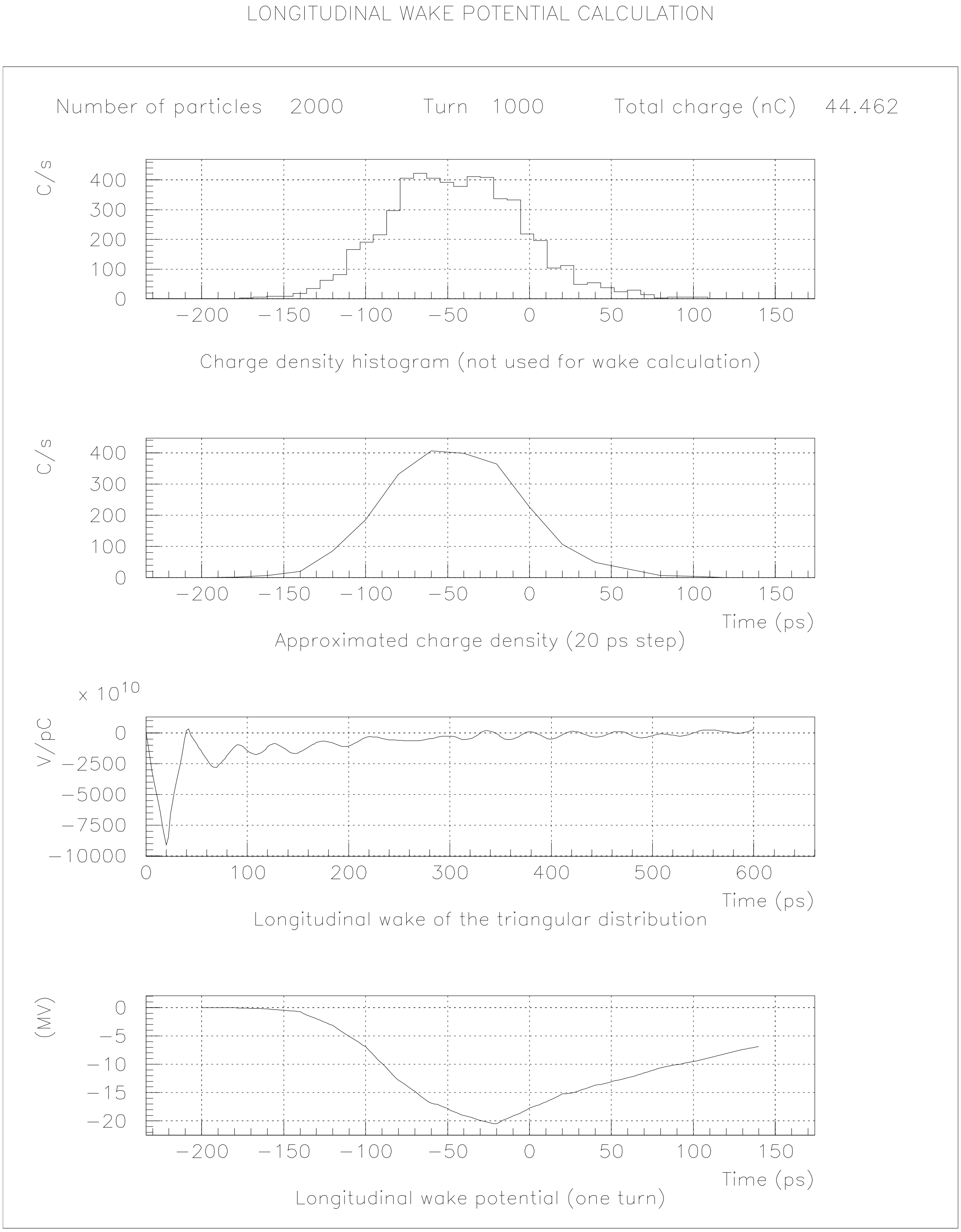

Figure 5: Calculation of the longitudinal wake potential (Δ=20 ps).

3 The LEP impedance model

The ability to predict the machine performance in different configurations depends critically on the accuracy with which the impedance is known. For this reason, a quite detailed model of LEP impedance has been defined, with contributions from resonant cavities, separators, tapers and bellows of different kinds. The elementary impedances which have been taken into account are the following:

- One cell of the (5 cell) copper cavity[6].
- A four cell superconducting cavity.
- An electrostatic vertical (ZL) separator.
- A shielded bellows for interconnecting vacuum chamber sections in the arcs (elliptic cross section).
- Straigth section bellows (circular cross section): two types have been considered, type L (RF cavities), type S (other, excluding separators).
- A pair of superconducting cavity module tapers.
- A pair of separator bellows and tapers.

It should be pointed out, however, that various limitations and simplifications are still present in this model. In particular, only axially symmetric stuctures have been considered: this means that non axially symmetric components have been either removed (RF couplers and tuners, collimators, pick-ups, kickers) or represented as axially symmetric by rotating their vertical (minimal radius) cross section around the beam axis (elliptic bellows, ZL separator electrodes); moreover, it has been supposed that all the elements are perfectly aligned with respect to the beam axis.

These simplifications are unavoidable in the present study, because they are already implied by the choice of a 2D representation of the beam dynamics. Their impact on the accuracy of the model is nevertheless expected to be relatively small. For what concerns the shielded bellows in the arcs, the possibility of replacing their elliptical cross section with a circular one, taking a radius of the same length as the vertical (short) axis, has been investigated by Y. Chin, using the 3D code WELL [16]: the difference in the transverse (vertical) loss factor between the elliptical and the circular representations of the cross section has been shown to be within a few per cent [17]. In the case of the vertical separators, a similar study has been carried out by G. Li, using the 3D code MAFIA [18] and the 2D code ABCI [19] to compare the transverse (vertical) loss factor of the planar electrodes geometry with that obtained by replacing the plates with a cylinder of the same radius as the half-width of the gap: the difference has been found to be below 10% [20]. Another simplification in the separator geometry has been the reduction of the length of the plates from 4 meters to 30 cm. The dependence of the loss factor on the length of the plates has also been investigated and found to be small, as far as the length of the plates is longer than the range of the wake potential calculation: the reason for this is that the electromagnetic field moving together with the beam does not change as the beam travels into the sandwich of the plates.

[6] Taking into account a single cell permits a reduction of the integration domain and of the CPU time required. This is possible in the case of the copper cavities beacause, due to the presence of the nose cones, the cells are well decoupled with respect to each other in the case of a short range excitation.

Other small 3D structures like pick-up buttons, collimators, couplers and tuners are only relevant to the stability of very short bunches [21]. The same argument holds for the contribution of non perfectly aligned elements. Larger objects, like feedback kickers, horizontal (Pretzel) separators, septum magnets, etc. are only few and can be neglected as well.

It should also be noted that for each impedance class which has been taken into account, different versions of the structure can exist, with slightly different geometries, while in the impedance model only one representative geometry for each class has been considered. The global error due to all these simplifications will be evaluated *a posteriori*, by comparing the predicted threshold current with the measured one. In principle, some underestimation of the total impedance is foreseeable, due to the various contributions which have been neglected.

The wake field calculations have been carried out with the code ABCI [19], which solves Maxwell equations in an axially symmetric structure using the FDTD (Finite Difference Time Domain) technique [22]. ABCI presents some advantages with respect to similar FDTD programs [23, 24, 25]: the implementation of a "moving mesh" permits to reduce the number of mesh points which have to be stored in memory if the range of the wake potential calculation is smaller than the length of the structure; a special integration method [26] improves the calculation of wake potentials in structures such as separators and collimators, in which parts of the boundary extend below the beam port radius; the use of triangular mesh cells in the boundary, the possibility of chosing mesh sizes different in the axial and radial directions, and the possibility of defining radial intervals, in which different mesh sizes are used, help for a better fitting of the mesh to the structure and permit to reduce the total number of mesh points; ABCI also permits a structure with "islands", i.e. areas detached from the main body, such as separator electrodes. All these features have been extensively used in the calculation of the wake potentials in the LEP impedances: figures 6, 7, 8, 9, report some examples of the discretized geometries which have been used to represent the geometry of the structures in the ABCI code.

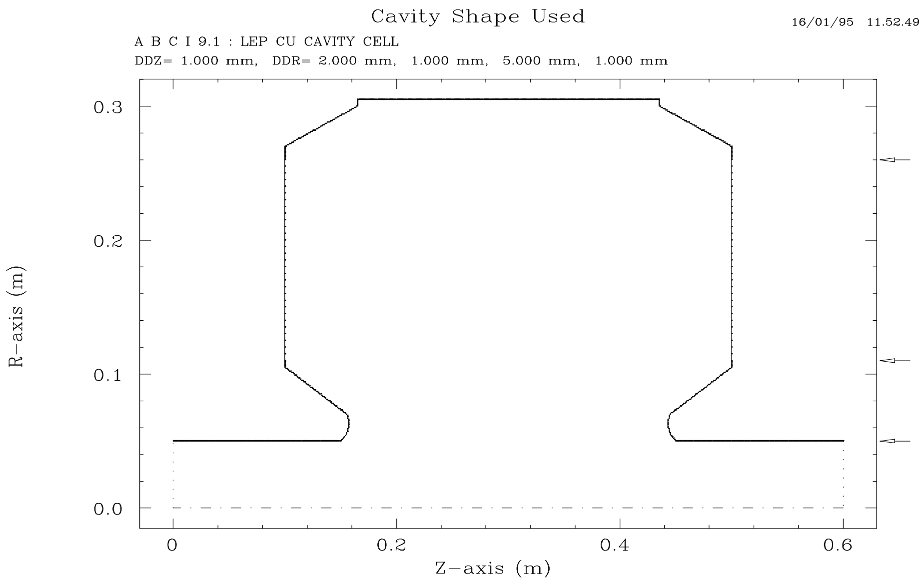

Figure 6: Discretized section of a copper cavity cell.

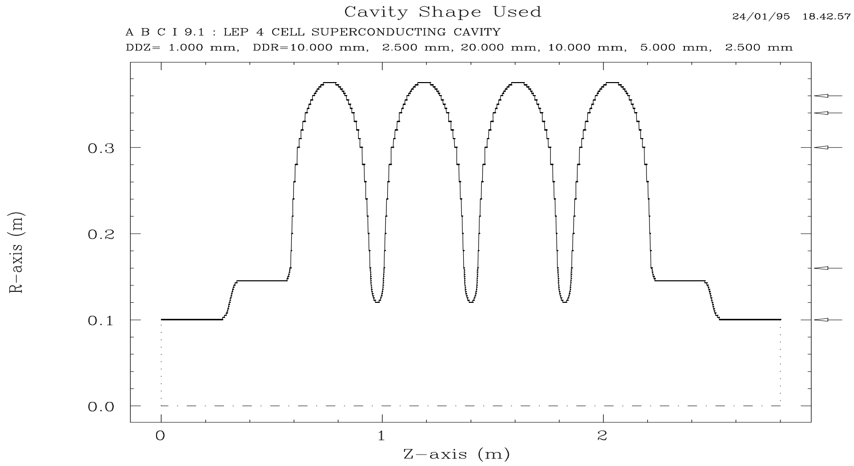

Figure 7: Discretized section of a four cell superconducting cavity.

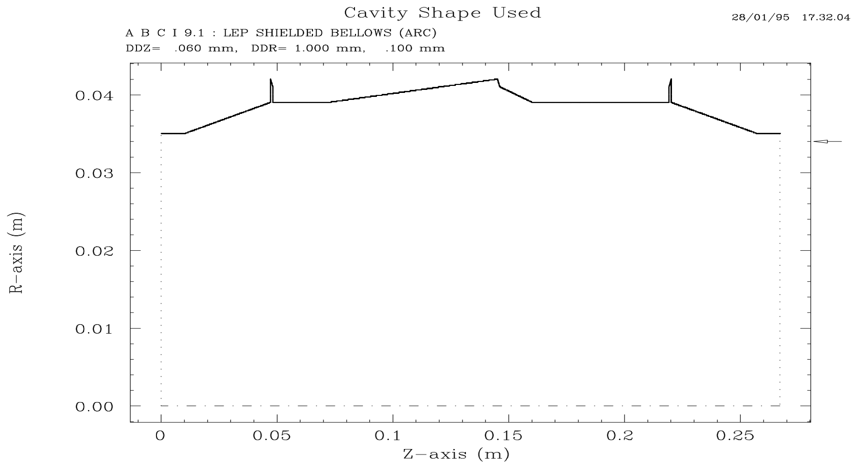

Figure 8: Discretized section of the sliding contacts of a shielded bellows (arc).

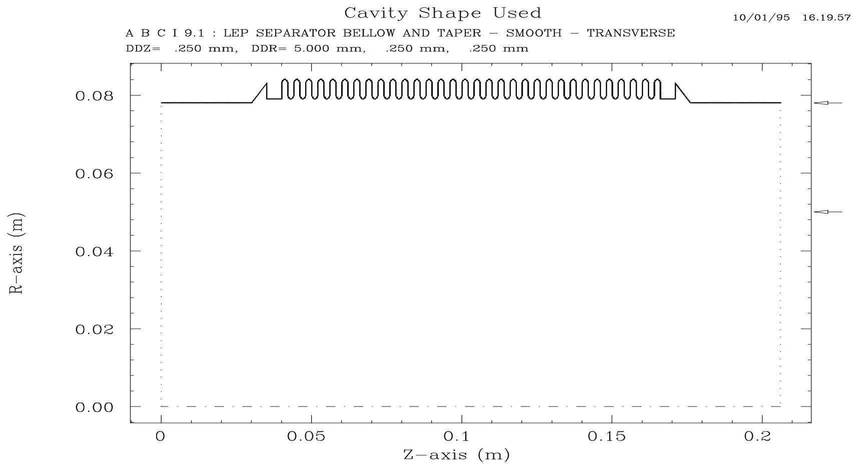

Figure 9: Discretized section of one separator bellows. This is a zoom over one part of the structure which has actually been considered; the full structure is composed by two such bellows and a pair of left-right tapers.

The impedance calculation in each structure has been first carried out for the case of Gaussian distributions of different length: the so obtained loss factors can be used to estimate how the total LEP impedance is shared by the various impedance classes, to build broad band resonator models of the impedance, to check the accuracy of the calculation of the basis functions wake potentials which are needed by the multi-particle tracking program (see section 4), and to estimate the TMC threshold by means of approximate formulae (see section 7).

Figures 10 and 11 report the results relative to the transverse loss factor of a Gaussian distribution as a function of bunch length, for the various basic structures which have been taken into account in the model.

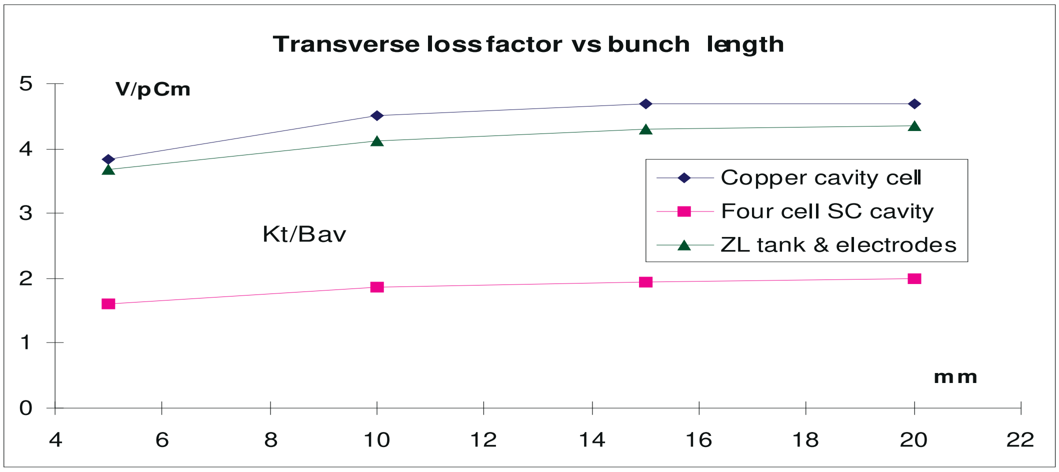

Figure 10: Dependence of the transverse loss factor of a Gaussian distribution on the rms bunch length (impedances with a low characteristic frequency).

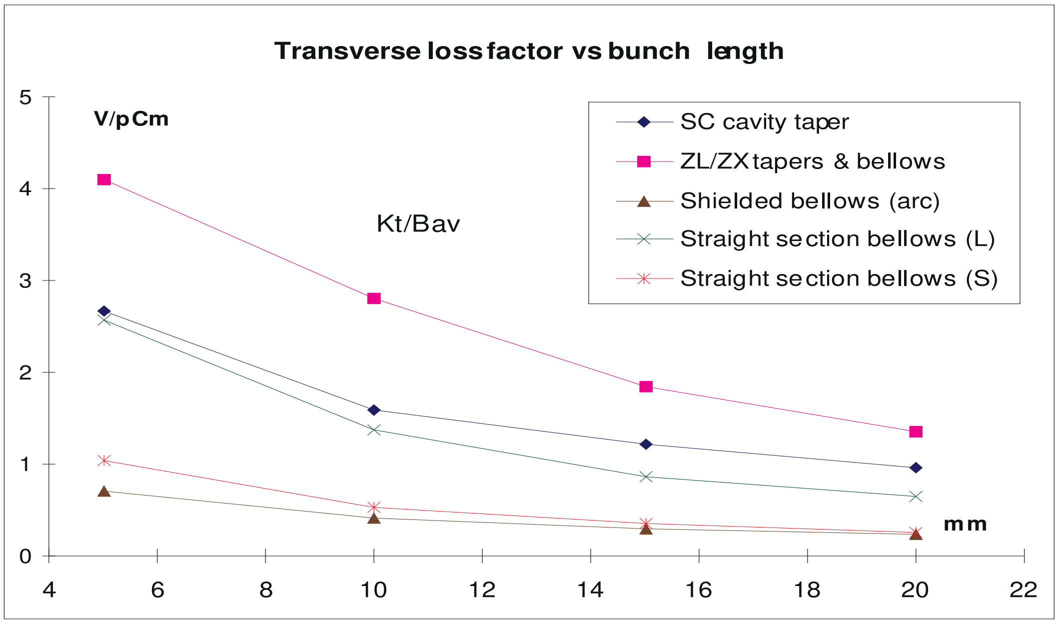

Figure 11: Dependence of the transverse loss factor of a Gaussian distribution on the rms bunch length (impedances with a high characteristic frequency).

The loss factors increase with bunch length for the structures of the "cavity" type, while they decrease with bunch length for the structures of the "bellows" type. This is because the resonant frequencies of the associated broad band resonators, as compared to the bunch spectrum, are relatively low (a few GHz) in the first case, due to the rather large dimensions of the gap and the beam tube, while they are quite large (tens of GHz) in the case of small corrugations of the beam pipe [14].

The effective loss factor relative to each class is then obtained by multiplying the loss factor of a single element by the number of elements installed, and, in the transverse (vertical) case, by scaling linearly with the average (vertical) β function at the elements. The result is therefore dependent on the optics: table 1 shows an example of this calculation, for the vertical loss factors in the LEP 90/60 (1994) optics, and for a rms bunch length of 1 cm. The resulting total vertical loss factor, normalized to the average vertical β function value of 56.4 m, is 4180 V/pCm.

Structure	N	β_y [m]	$K_\perp$ [V/pCm]	$N\beta_y K_\perp/\beta_{av}$ [V/pCm]
Copper cavity cell	600	40.6	4.519	1951.8
Four cell SC cavity	20	51.3	1.894	34.4
ZL tank & electrodes	36	66.4	4.272	181.1
Shielded bellows (arc)	2668	84.8	0.419	1682.8
Separator tapers & bellows	47	56.1	2.874	134.3
Straight section bellows (L)	128	40.6	1.373	126.5
Straight section bellows (S)	160	40.6	0.532	61.2
SC module taper	5	51.3	1.737	7.89

Table 1: Contributions to the transverse (vertical) loss factor for a Gaussian distribution of 1 cm rms length (one complete revolution). The β function values are those corresponding to the LEP 90/60 (1994) optics. The loss factors are normalized to the average β function value in the ring (β_{av}=56.4m). The average values of the β function at the cavities and in the arcs have been computed by A. Verdier.

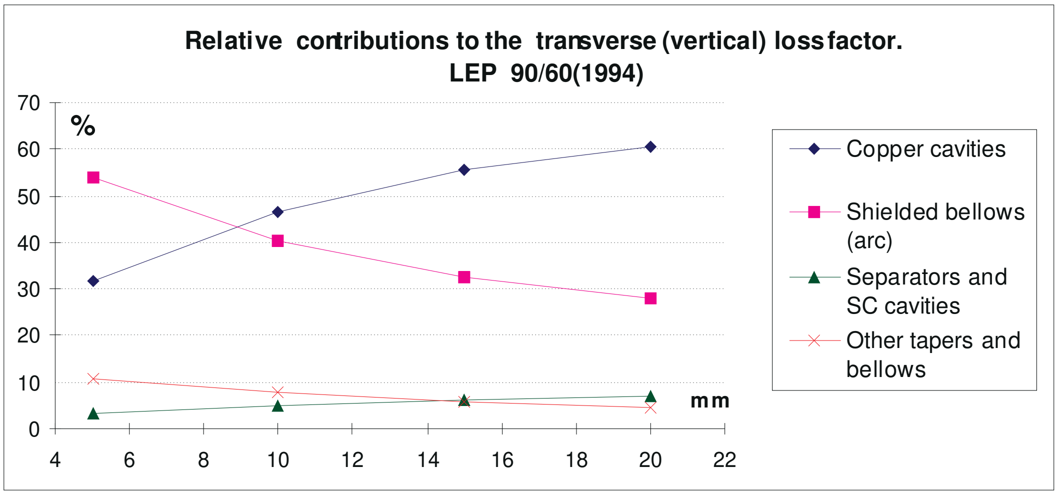

Figure 12: Relative contribution to the total impedance of the different impedance classes which have been considered in the model, as a function of bunch length (LEP 90/60 1994 optics).

Figure 12 shows the relative (per cent) contribution of each class to the total vertical impedance as a function of bunch length, again for the case of the LEP 90/60 (1994) optics: the major contributions to the transverse impedance come from the copper cavities and the shielded bellows, mainly due to their large number. It is again worth noting the already mentioned strong dependence of the relative weight of the different impedances on the bunch length.

By repeating the calculation of table 1 for different values of the bunch length, and by taking the average values of the (vertical) β functions for the different optics of interest, the dependence of the total (vertical) loss factor on the bunch length can be found: the result is reported in figure 13.

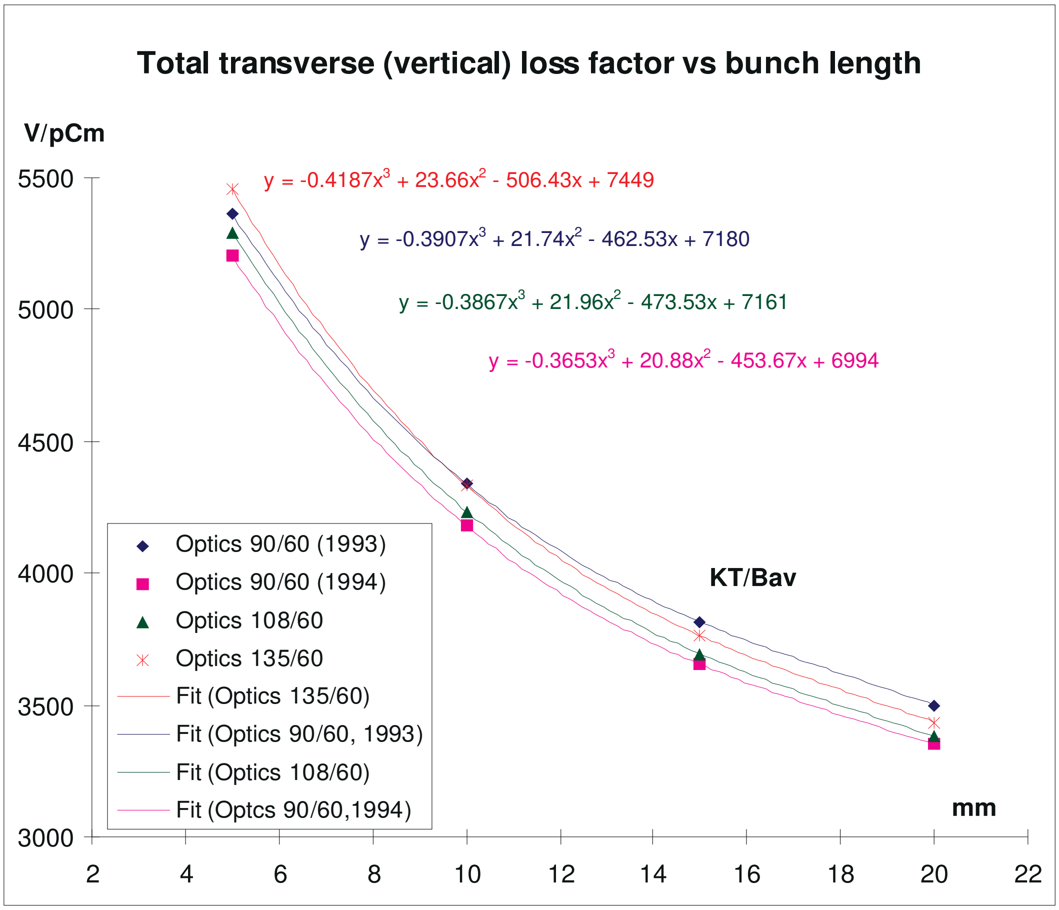

Figure 13: Dependence of the total vertical loss factor on the rms bunch length for different LEP optics.

An estimation of the threshold for the transverse mode coupling instability, which is the main single-bunch intensity limitation at LEP, can be obtained from the curves of figure 13 by evaluating the approximate expression [28]:

$$I_{th} = \frac{8 f_s E/e}{\sum_i \bar{\beta}_i k_{\perp i}(\sigma_s)} \tag{14}$$

where f_s is the synchrotron frequency, and E is the operating energy.

This method will be applied in section 7 to various configurations of the LEP machine, and the results will be compared with those obtained by the multi-particle tracking program, and with the experimental data.

For what concerns the longitudinal impedance, table 2 reports the longitudinal loss factors for a Gaussian distribution of 1 cm rms length. Both the loss factors relative to one element of each of the impedance classes, and the ones relative to a complete revolution, are reported. The total one-turn loss factor is 425.4 V/pC.

Structure	N	$K_{\parallel}$ [V/pC]	$-NK_{\parallel}$ [V/pC]
Copper cavity cell	600	-0.5712	342.72
Four cell SC cavity	20	-1.087	21.18
ZL tank & electrodes	36	-0.5096	18.345
Shielded bellows (arc)	2668	-0.008	23.297
Separator tapers & bellows	47	-0.311	14.617
Straight section bellows (L)	128	-0.03188	4.080
Straight section bellows (S)	160	-0.01017	1.627
SC cavity taper	5	-0.1815	0.907

Table 2: Longitudinal loss factors for a 1 cm rms Gaussian distribution.

In the longitudinal plane, the copper cavities have the dominant loss factor: at 1 cm, they alone contribute over 80%; the contribution of the bellows to the total loss factor becomes important only for very short bunches, as shown in figure 14.

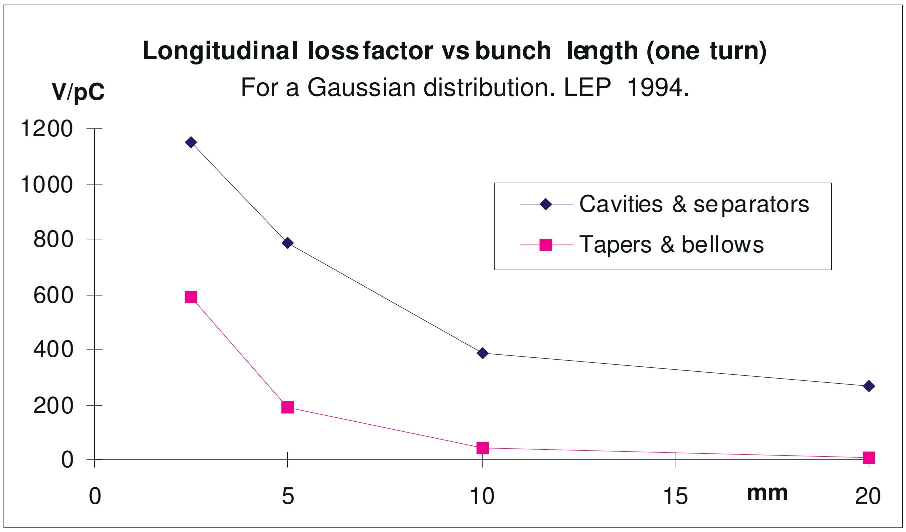

Figure 14: One-turn longitudinal loss factors as a function of bunch length.

It should be pointed out, however, that the loss factor is not always a good indicator of the effect produced on the bunch by a given structure. This is the case, in particular, of the impedances with a high characteristic frequency: here the longitudinal loss factor tends to zero for sufficiently long and symmetric distributions, because the wake potential becomes proportional to the first derivative of the charge distribution function, as shown in figure 16.

This leads to an almost exact cancellation of the loss factors relative to the head and the tail of the bunch, which means that the net energy balance for the bunch is zero; however, the loss factors relative to the head and the tail of the bunch, when taken separately, are not small. This rapidly oscillating component of the longitudinal wake potential can produce important effects: in particular, as it will be shown in chapter 7, the “bellows” can play an important role in the bunch lengthening and in the onset of longitudinal turbulence.

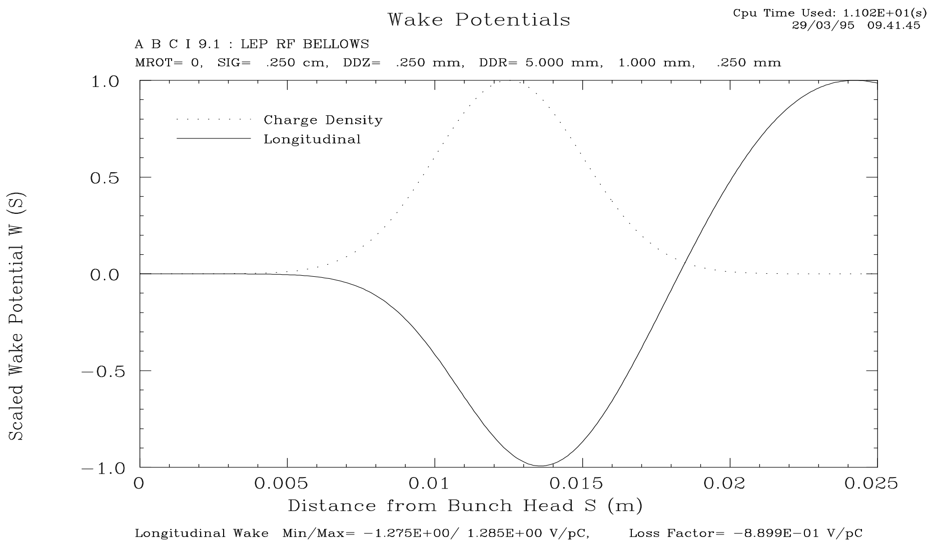

Figure 15: LEP RF bellows: longitudinal wake potential for a Gaussian distribution of 2.5 mm rms length.

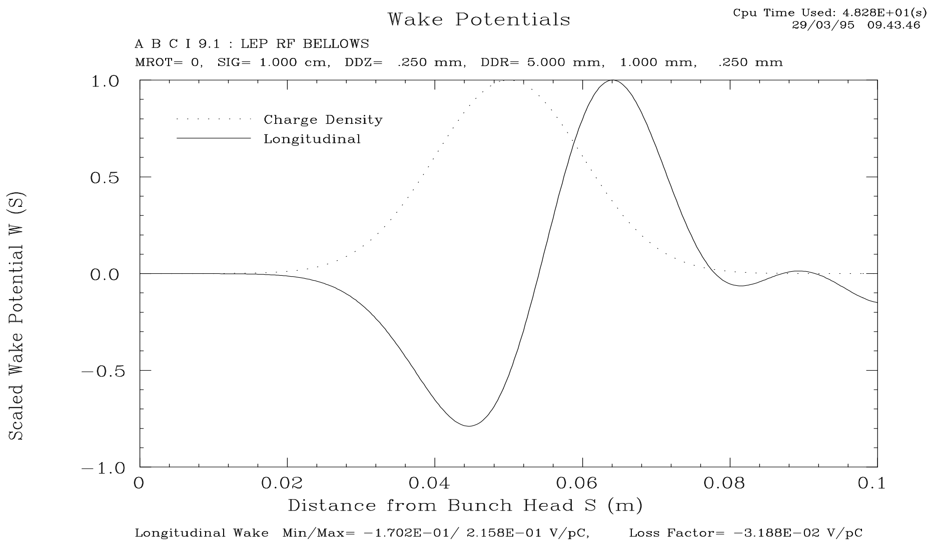

Figure 16: LEP RF bellows: longitudinal wake potential for a Gaussian distribution of 10 mm rms length.

4 Calculation of the reference wakes

The calculation of the reference wake potentials, i.e. those generated in the LEP impedances by the distribution used as basis function in the multi-particle tracking program, has been carried out with the mesh code ABCI [19], which can rather easily handle distributions of non-Gaussian longitudinal shape[7]. ABCI computes the wake potential generated by a hollow beam of the form:

$$j(s) = \frac{c}{2\pi b} f(s - ct)\delta(r - b)\cos(m\theta)$$

where $f(s)$ is the longitudinal density, given in the present case by equation (8), and b is the radius of the hollow beam, which is generally chosen equal to the beam pipe radius.

Two possible choices of the basis function have been considered, with a half-width of 10 ps (3mm) in the first case, of 20 ps (6mm) in the second case. The wake potential calculation has been extended to a distance of, respectively, 15 and 30 cm behind the distribution. According to the discussion in section 2.2, the first basis function can be used when the rms bunch length is between 6 and 15 mm, the second one for rms bunch length between 12 and 30 mm.

The structures which have been taken into account are those of the impedance model described in section 3, and the geometries are the same which have been used for the calculation of the loss factors of Gaussian distributions, but with smaller mesh sizes, in particular in the longitudinal direction.

The reason for smaller mesh sizes is that the Fourier spectrum of the basis distributions with Δ=10-20 ps is centered, respectively, around frequencies of the order of 20-10 GHz, to be compared with frequencies of 2-1 GHz for Gaussian distributions with rms length of, respectively, 1-2 cm. Moreover, due to the discontinuities in the first derivative, the Fourier spectrum of the triangular shaped distribution is less peaked on the characteristic frequency than the one of the smoother Gaussian distribution: the triangular distribution has then significant Fourier components in the high frequency region of the spectrum, and for this reason can excite, in the cavity, higher order resonant modes. In cases in which also the cavity impedance has significant high frequency components, it will be necessary to chose a mesh step which is sufficiently small to correctly represent these higher order, rapidly oscillating modes. This is especially true for the smaller "cavities", that is the bellows and the tapers.

The calculation of the response of the structure to high frequency excitations is, on the other hand, essential to the simulation program, because such excitations are an important aspect of the higher current beam dynamics and have then to be correctly represented. In this respect, the difficulties encountered in the calculation of the wake potential of a triangular shaped distribution can be correlated to those encountered in the calculation of the wake potential of the higher order Hermite polynomials (program HERSIM [3]), or to those emerging in evaluating the wake function of a point charge (program SIMTRAC [4]). As compared to the Hermite polynomials, the linear interpolating functions present the disadvantage of having discontinuities in the first derivative, while they are better in representing strongly non-Gaussian distributions, and allow for a simpler and faster calculation.

The accurate calculation of the wake potential due to a distribution with high frequency Fourier components can be a rather demanding task. In this respect, the FDTD method, which

[7] The calculation of the wake potential due to a triangular shaped distribution has been anyhow included as a standard feature of ABCI, starting from version 8.7.

belongs to the family of the finite difference methods, presents serious limitations, which can be related to an insufficient flexibility in the type of mesh which can be used to discretize the problem. In fact, finite difference methods are in practice limited to regular, or quasi-regular, meshes. On the contrary, it would be extremely useful to locally vary the mesh density throughout the field, i.e. increase the mesh density in areas of rapidly changing field, and decrease it in areas of slowly changing field, thus enhancing the ratio between the achieved accuracy and the computational effort. The Finite Element Method (FEM) offers great flexibility in the choice of the mesh [30]. This also allows for a better representation of the geometry of the problem, which can be further enhanced by the use of second order isoparametric elements for fitting curved boundaries.

The application of the Finite Element Method to compute transient electromagnetic fields in accelerating structures was already suggested by A. Khursheed in 1987 [29]; an example of a FEM program for wake field calculations is the PRIAM/ANTIGONE package [31]. However, finite difference codes have been more successful in wake field calculations, probably because they are simpler to formulate and require less programming effort. As a result, many well tested and well documented FDTD programs [18, 19, 23, 24, 25] are available to the accelerator community: this is why an FDTD program has been chosen for the wake potential calculations in the present study. Good results can be obtained with the FDTD method in the calculation of the wake potentials in axially symmetric structures; the FEM method will probably be required to perform accurate calculations in fully 3D structures.

Structure	Δ	$\Delta/\delta z$	Nz	Nr	CPU (h)	
	ps		(structure)		m=0	m=1
Copper cavity cell	10	50	10008	156	7.5	10.3
	20	50	5004	156	3.3	3.9
Four cell SC cavity	10	60	56040	58	11.6	10.6
	20	60	28020	58	5.9	5.8
Arc shielded bellows	10	120	10687	98	5.0	4.7
	20	120	4453	98	2.3	1.6

Table 3: Calculation of the reference wake potential in the main LEP impedances. The calculation has been carried out on an HP-UX 9000/735 workstation.

Table 3 reports the data relative to the mesh sizes which have been used for the reference wake potential calculation in the structures which are responsible for the main contributions to the total impedance: the copper cavities (80% of the longitudinal loss factor and 30-50% of the transverse loss factor), the shielded bellows of the arcs (30-50% of the transverse loss factor) and the superconducting cavities, which are important for LEP2 studies. For simplicity, the same mesh has been usually chosen in the calculation of the longitudinal and of the transverse wakes, but two independent meshes could also be used. The calculations presented in table 3 present different characteristics: the superconducting cavity requires a long CPU time, due to its large integration volume; the shielded bellows requires a small mesh size, due to its very high frequency spectrum; the copper cavity cell, which has a relatively small integration volume and a relatively low frequency spectrum, does not pose any particular problem to the reference wake potential calculation: however, since this structure represents the main contribution to the impedance, a fine mesh has also been used in order to obtain an accurate representation of the geometry.

The results of the the wake potential calculations for the shorter basis function (Δ=10ps) are shown in figures 17 and 18.

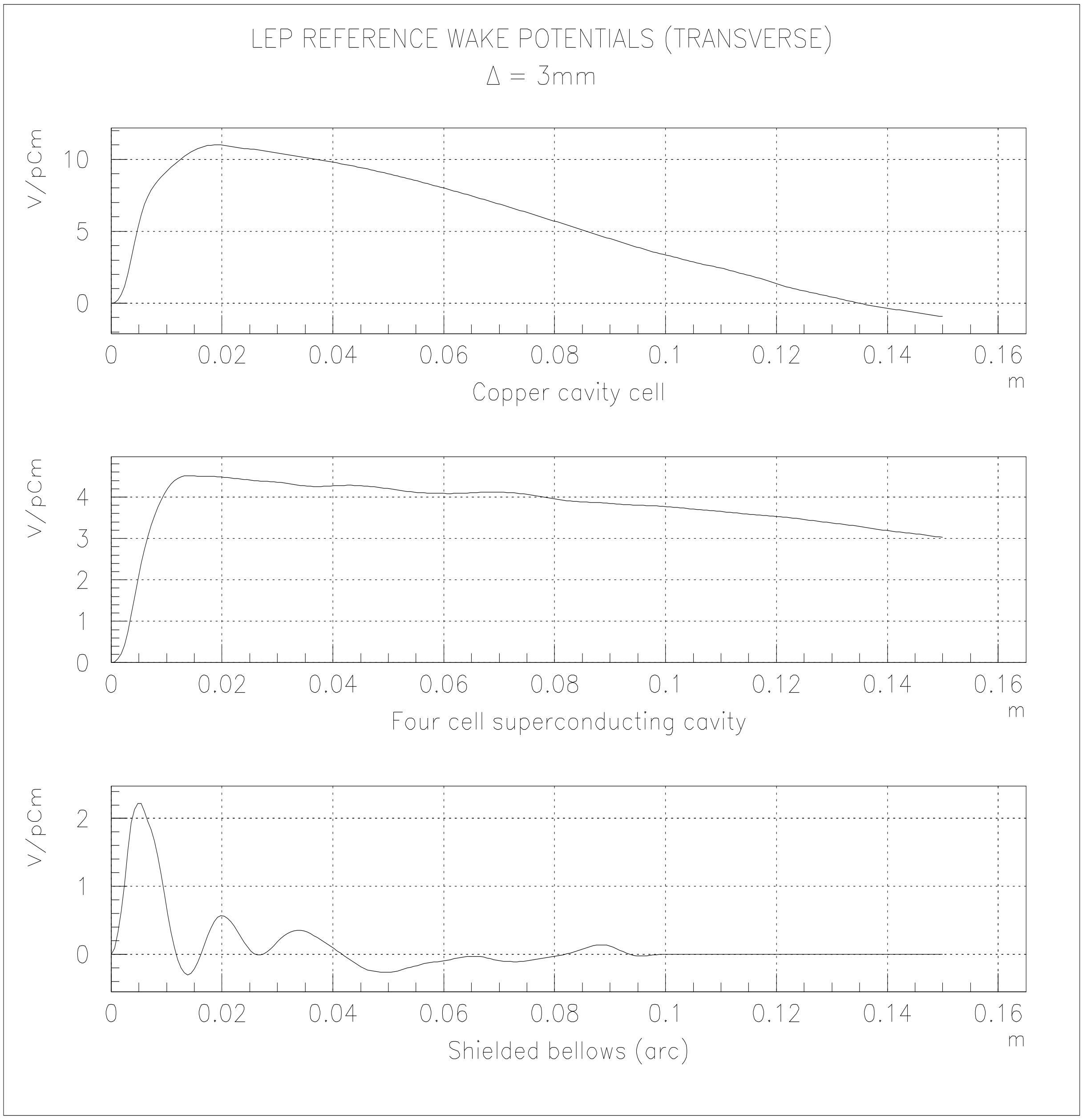

Figure 17: Transverse wake potentials for the Δ=10 ps basis function in the main LEP impedances.

In order to check the accuracy of the wakefield representation, one can compare the wake potential of a Gaussian distribution, computed by ABCI, with that obtained by expanding the Gaussian distribution on the basis of linear interpolating functions, and adding up the contributions from each element of the expansion. Figure 19 reports an example of such a comparison: here a LEP RF cavity cell is considered, and a 50 ps (15mm) rms Gaussian distribution is expanded as sums of linear interpolating functions with Δ=20 ps (6mm). As can be seen, it is difficult to distinguish the two curves from each other. It should be noted that in such a comparison two separate sources of errors are present: the first is the error in the representation of the distribution by the piecewise linear approximation, the second is the error in the calculation of the basis function wake (high frequency spectrum, discontinuities in the first derivative).

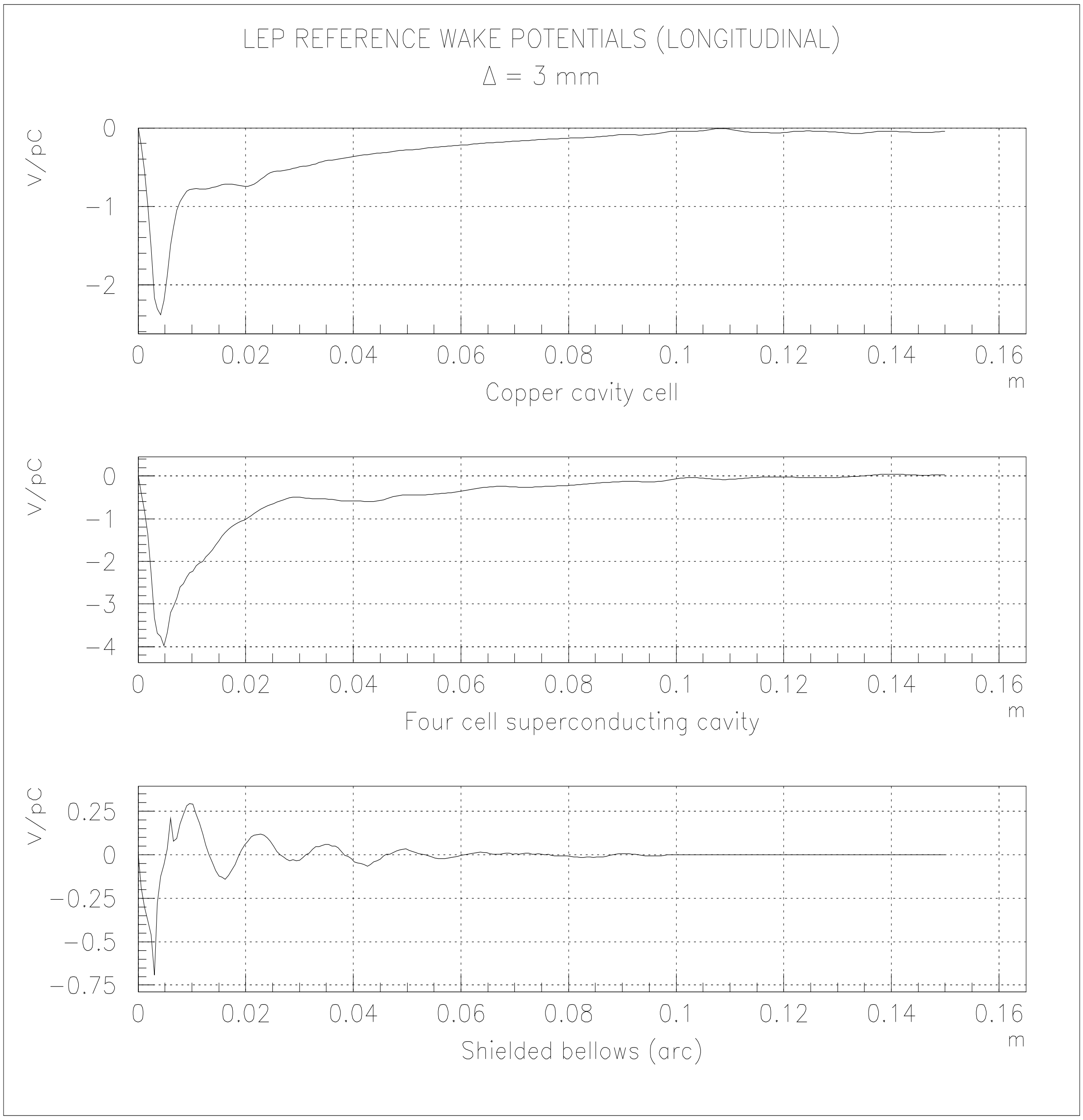

Figure 18: Longitudinal wake potentials for the Δ=10 ps basis function in the main LEP impedances.

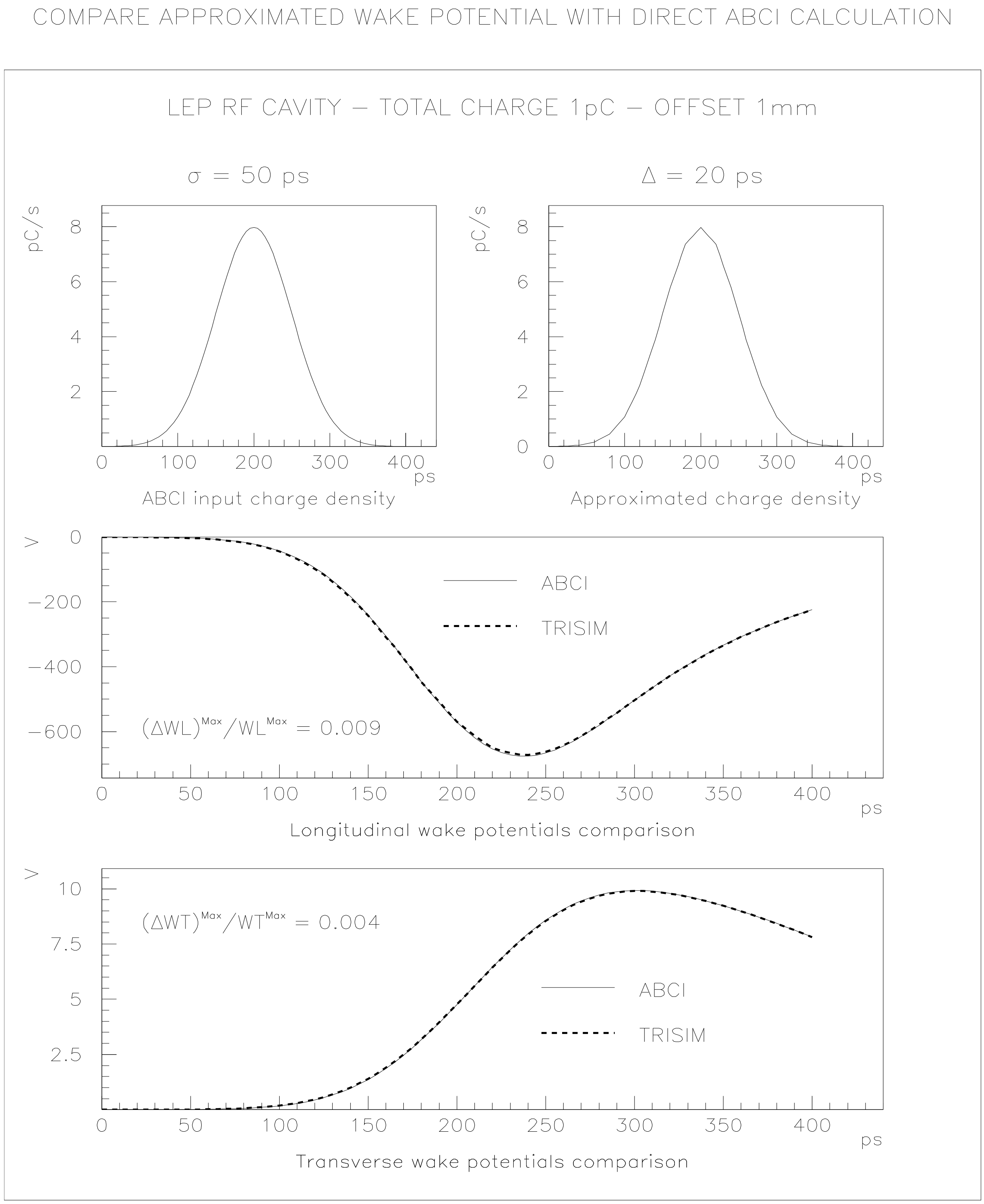

Figure 19: Comparison between the wake potential of a Gaussian distribution computed with ABCI and that obtained by expanding the distribution as sums of linear interpolating functions.

The maximum relative difference in the longitudinal wake potential calculation, normalized to the maximum absolute value of the wake potential, is in this case only 0.9%. However, it has been found that for some structures (bellows) the errors were larger in a few points, namely those corresponding to the s_k positions of figure 1. This is because, for the reasons which have already been explained, the calculation of the wake potential at the position of the vertex of the triangular basis function is not very accurate. It has therefore been decided to replace the wake potential values obtained, in the s_k positions, by the formula (12), with a linear interpolation between the closest points. This correction is included in the all the comparisons which are presented in what follows, and in the simulation program, as far as the longitudinal wake is considered. In the case of the transverse wake, this problem did not appear.

Structure	Δ=10ps & σ=1cm		Δ=20ps & σ=2cm	
	$\delta K_{\parallel}/K_{\parallel}$ %	$\delta K_{\perp}/K_{\perp}$ %	$\delta K_{\parallel}/K_{\parallel}$ %	$\delta K_{\perp}/K_{\perp}$ %
Copper cavity cell	0.21	0.67	0.34	0.28
Arc shielded bellows	0.75	1.86	1.19	0.98
SC cavity (4 cells)	0.62	1.43	0.28	1.53

Table 4: Relative errors in the loss factors of a Gaussian distribution expressed as sums of linear interpolating functions, by making use of the reference wake potentials for the Δ=10ps and the Δ=20 ps basis functions, and comparing with the loss factors obtained with a direct ABCI calculation.

Table 4 reports the relative errors for the longitudinal and transverse loss factors of the Gaussian distribution expressed as sums of linear interpolating functions. In all the cases which have been examined, the error is below 2%. The best results are obtained for the copper cavities, while less good results are obtained for the shielded bellows. Taking into account that the wake potential calculation in the bellows is not very demanding in terms of CPU time, one could consider the possibility of performing a more accurate calculation with a finer mesh. However, it should be noted that the wake potential in the bellows is the result of a superposition of high frequency resonant modes, and that these modes critically depend on small variations of the geometry. Using different FDTD meshes, different representations of the geometry are obtained, and the solutions, each correct with respect to the corresponding representation of the boundary, can differ of one or two per cent with respect to each other. From the mathematical point of view, one solution would consist in adopting a discretization method like the FEM, where the geometry representation can be made independent of the the mesh size (at least for sufficiently fine meshes). From the physical point of view, however, it should be recalled that there are about 2700 such bellows in the machine, all different from each other due to the fabrication tolerances, and in time due to temperature variations. A higher degree of uncertainty in the knowledge of the wake potential in the bellows should therefore be regarded as intrinsic to the physics of this structure.

For what concerns the average error, it can be estimated by adding up the reference wake potentials corresponding to the 8 classes of structures which have been taken into account, and by scaling with the number of installed elements in each class and with the average β function values, so to obtain an "effective" one turn wake. This wake can be used to compute the one-turn loss factor of a Gaussian distribution expressed as sums of linear interpolating functions, which can be compared with that obtained from a direct ABCI calculation, as it was done in tables 1 and 2. The results of this comparison are shown in table 5.

Relative error %	σ=1cm Δ=10ps	σ=2cm Δ=20ps
$\delta K_{\parallel}/K_{\parallel}$	-0.04	-0.4
$\delta K_{\perp}/K_{\perp}$	+1.3	+0.6

Table 5: Errors in the one-turn loss factors of a Gaussian distribution expressed as sums of linear interpolating functions. Optics 90/60, 1994.

Following the results in tables 4, 5, it can be concluded that the inaccuracies in the calculation of the reference wake potentials for the triangular-shaped basis function do not affect significantly the simulation of the beam dynamics. In fact, other sources of error are expected to be dominant:

- The simplifications in the geometry of the structures which have been taken into account, and the contributions from all the structures which have not been taken into account, in particular for what concerns 3D effects.
- The imperfect representation of the physical reality given by the macroparticle distribution, and the resulting uncertainty in the calculation of the distribution moments. This effect, which is mainly due to the use of a limited set of macroparticles, is probably the major source of error in the beam dynamics simulation.

Table 3 also reports the CPU time which has been required for the calculation of the reference wakes on an HP 9000-735 workstation. With each calculation in the range of 2-10 hours of CPU, and 32 different calculations to perform (8 elementary structures, 2 basis functions, longitudinal and transverse wakes), the total number of CPU hours which have been necessary for the reference wake calculation is around 140. This effort was considered to be a good investment in order to obtain an accurate impedance model, which can then be used for many beam dynamics studies. At the same time, this exercise allowed to investigate the feasibility of calculating the wake potential of a triangular shaped function in a wide variety of structures.

It should be pointed out, however, that useful impedance models in terms of linear interpolating functions can also be obtained with much less computational effort. For what concerns the number of structures taken into account, usually a few impedance classes (in the case of LEP, the copper cavity and the bellows) contribute to most of the impedance, so that all the other contributions can be neglected in many applications. For what concerns the CPU time which is needed for obtaining a single reference wake, the use of a coarser mesh allows for a much faster calculation, of the order of some minutes, as shown in figure 20 for the case of a LEP bellows: in this case, the comparison between the loss factors would give a relative error around 10-15%, which can also be accepted in many applications. The calculation of the reference wakes for two basis functions of different length was carried out mainly in order to investigate the stability of the results with respect to Δ. However, at least in the case of LEP, one basis function would be enough to cover the range of bunch length of interest in most applications.

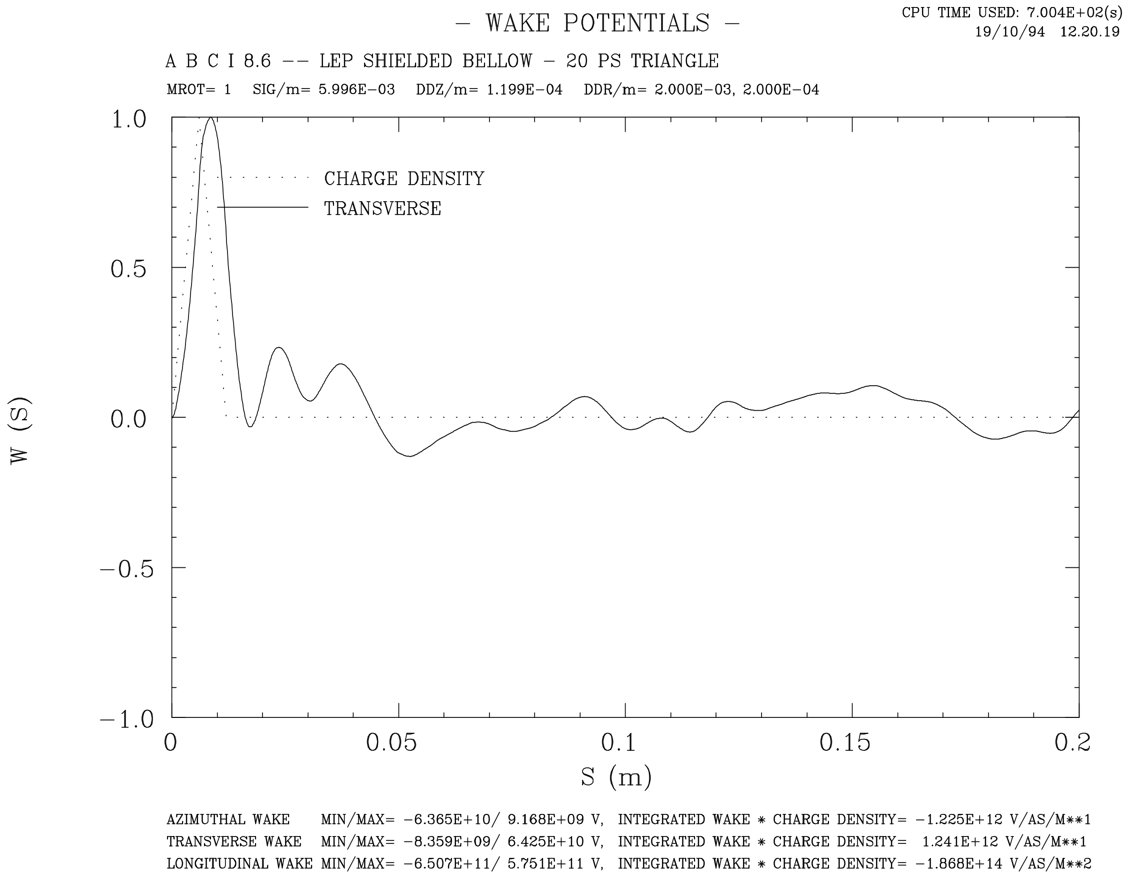

Figure 20: Calculation of the wake potential for a triangular shaped distribution (Δ=20 ps) in a LEP bellows, using a coarse mesh. The wake potential is that corresponding to a total charge of 1C and to a transverse displacement of 3.5 cm (tube radius).

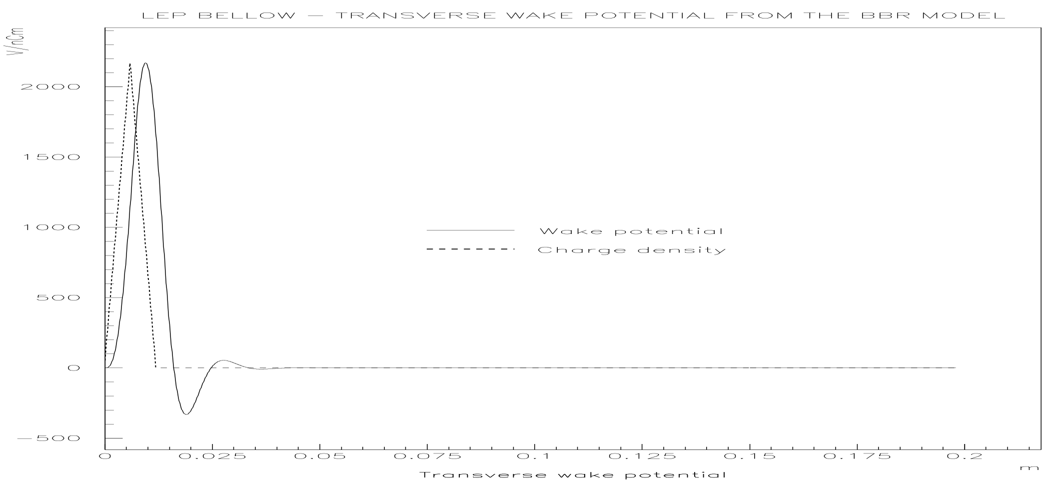

Figure 21: Calculation of the wake potential for a linear interpolating function (Δ=20 ps) in a LEP bellows, from the BBR parameters (16).

An alternative, fast technique for the calculation of the reference wakes can be used if a sufficiently accurate model of the impedance in terms of broad band resonators (BBR) is available. This means that the actual impedance, which is usually a very complicated function of frequency, with many sharp peaks due to the resonant modes, is replaced by a superposition of (a few) contributions, each of them corresponding to the impedance of a single mode cavity with a low quality factor Q. For example, the transverse impedance (per unit displacement) can be written:

$$Z_\perp(\omega) = \frac{\omega_r}{j\omega} \; \frac{R_\perp}{1 + jQ\left(\omega/\omega_r - \omega_r/\omega\right)} \tag{15}$$

This description of the impedance can be used in single bunch stability studies, because the details of individual sharp resonances are not resolved in the short time of a bunch passage. It permits the characterization of the whole impedance function by only three parameters: resonant frequency, shunt impedance and quality factor. A second advantage is the fact that an explicit evaluation of the integrals which are involved in the calculation of stability limits or growth rates is made possible. From the point of view of the multi-particle simulation studies, however, the interest in the use of a BBR model derives mainly from other considerations:

- Using a BBR model of the impedance, it is possible to solve equation (5) in order to obtain the wake potential of the basis functions, both for the Hermite polynomials and for the linear interpolating functions. The so obtained wake potentials are equivalent in the frame of the chosen approximation, as they are not affected by the different sources of errors which are present when the wakes are derived from a numerical solution of Maxwell equations (numerical derivations for the Hermite polynomial wakes, excitation of higher order resonances for the linear interpolating functions). The broad band model allows then for a consistent comparison between the two wakefield representation methods. The same is true for evaluating the stability of the representation in terms of linear interpolating functions with respect to the choice of the parameter Δ, using two equivalent reference wakes.
- The BBR model, which allows for an easier and faster calculation of the reference wakes with respect to an electromagnetic analysis code, can be used to perform preliminary calculations, or in general purpose studies, not related to any specific machine, or for checking the wakes obtained by numerical solution of Maxwell equations.

Unfortunatly, the determination of a BBR model which fits to a sufficient accuracy the actual impedance is not always straightforward. In the case of LEP, for example, it was not possible to obtain a useful BBR model of the longitudinal impedance [15]. On the contrary, for what concerns the transverse plane, it has been shown that a rather accurate description of the impedance of LEP can be obtained with a model based on two broad band resonators (corresponding respectively to the copper cavities and to the bellows), the parameters of which are [14, 15]:

$$\begin{array}{lll} f_r^{(\mathrm{cav})} = 2GHz & R_\perp^{(\mathrm{cav})} = 2.36k\Omega/m & Q^{(\mathrm{cav})} = 1 \\ f_r^{(\mathrm{bel})} \geq 12GHz & R_\perp^{(\mathrm{bel})} = 114\Omega/m & Q^{(\mathrm{bel})} = 1 \end{array} \tag{16}$$

Here the quoted shunt impedances are those corresponding to a single structure: the corresponding total values are $1.51\mathrm{M}\Omega/\mathrm{m}$ for the cavities, and $0.32\mathrm{M}\Omega/\mathrm{m}$ for the bellows.

The transverse wake function corresponding to the broad band impedance can then be obtained as [4]:

$$V_T^{m=1}(t) = \omega_r \frac{R_T}{Q'} exp(-\omega_r t/2Q) \sin(\omega_r' t) \tag{17}$$

where the following definitions have been applied:

$$\begin{aligned} Q' &= uQ && (18) \\ \omega_r' &= u\omega_r && (19) \\ u &= \sqrt{1 - \frac{1}{4Q^2}} && (20) \end{aligned}$$

and the wake potential for a general distribution can be obtained by solving the convolution integral (5).

The result of the calculation of the transverse wake potential in a LEP bellows for a basis function with Δ=6 mm, starting from the BBR parameters (16), is shown in figure 21; it can be compared with the wake potential of figure 20, which has been obtained with the ABCI program. From the qualitative point of view, it is apparent that the BBR model, while reproducing correctly the first oscillation of the wake potential, operates a quite drastic simplification of the physical reality after the first zero-crossing. A quantitative comparison between the two curves leads to the following results: the longitudinal position of the first zero-crossing is at 1.7 cm for the ABCI calculation, at 1.6 cm for the BBR model calculation; the maximum peak of 6.4 10^{10} V/C at a radius of 3.5 cm, computed with ABCI, corresponds to a normalized wake potential of about 1850 V/nCm, to be compared with a maximum value of about 2200 V/nCm obtained with the broad band model. The latter result is not very satisfactory: it should be noted, however, that the BBR parameters are optimized to fit the loss factor, rather than to fit the wake potential curve.

5 Model of the LEP machine

As it was already mentioned, the machine geometry is modelled, in the simulation program TRISIM, by a ring diveded into a given number of sectors, each one composed by a point-like element followed by an arc. The point-like elements represent structures, the effect of which can be modelled as a kick: in the study of collective effects, the most important structures which have to be taken into account are the accelerating cavities (with their associated RF voltage and impedance), the other impedances (which are defined in the program as cavities with zero RF voltage), and the feedback kickers. The main simplifications which are implied by this representation are the following:

- The length of the structures is assumed to be sufficiently short to be neglected.
- The motion in the arc is assumed linear.

Both these assumptions do not affect significantly the study of collective effects. In the case of a large accelerator like LEP, however, a third important simplification is necessary in order to obtain a useful machine model: the effects of many structures has to be concentrated into a relatively few point-like elements. This is necessary because the CPU time increases linearly with the number of elements (and arcs) which are present in the machine representation: although up to 100 elements can be defined, it is more reasonable to limit their number to less than 10. In any case, as it will be shown in what follows, more detailed machine models are not required in most applications.

As a general rule, it is possible to concentrate the effect of different structures in one element as far as the longitudinal position of the bunch particles (with respect to the synchronous particle) can be assumed constant in traversing from one structure to the other, i.e. as far as the distance between the structures is small compared with the length of a synchrotron oscillation. The derivation of this criterion is straightforward as far as longitudinal effects (RF acceleration and longitudinal impedance) are concerned; the case of the transverse wake is slightly more complicated as the kick produced by a leading particle on a trailing test charge depends on both the relative distance of the two charges and on the vertical position of the leading particle (see equation 2); however, since the two charges are performing betatron oscillations with the same frequency, successive kicks coming from a sequence of structures always add up linearly. For what concerns the averaging of the vertical kick strength due to the change of betatron phase of the leading particle when traversing the sequence of structures, in the simulation program this effect is accounted for by the averaging of the dipole moment distribution function over many particles with different betatron phase, and by averaging over successive passages through the point-like element at different turns.

In LEP, the synchrotron period is of the order of ten turns, so it should be possible to concentrate in a single point the effects of structures located at a distance of less than some fraction (say, one fifth) of the machine circumference. Since an exact criterion is not easy to formulate, two different machine models have been defined, one with four impedance elements, the second with 12 impedance elements, and the stability of the simulation results with respect to the choice of the machine representation has been investigated (see section 6.1). The first model is illustrated in figure 22, the second in figure 23: both models account for the presence of two symmetric accelerating stations around IP2 and IP6, and both of them have different elements to represent the impedance of the curved sections (shielded bellows) and that of the straight sections (copper and superconducting cavities, separators and the associated bellows and tapers). In both cases, a pick-up placed in IP1 (Start LEP) collects, at each turn, the relevant bunch parameters. In the second model, the impedance of the shielded bellows is further smeared along the arc, the presence of two separated accelerating stations on both sides of the IPs is accounted for, and the impedance of the copper cavities is separated from the rest of the straight section impedance. As it will be shown in section 6.1, the results obtained with the two machine representations are equivalent, so the first model, which permits a three times faster calculation, will be the one employed in most applications.

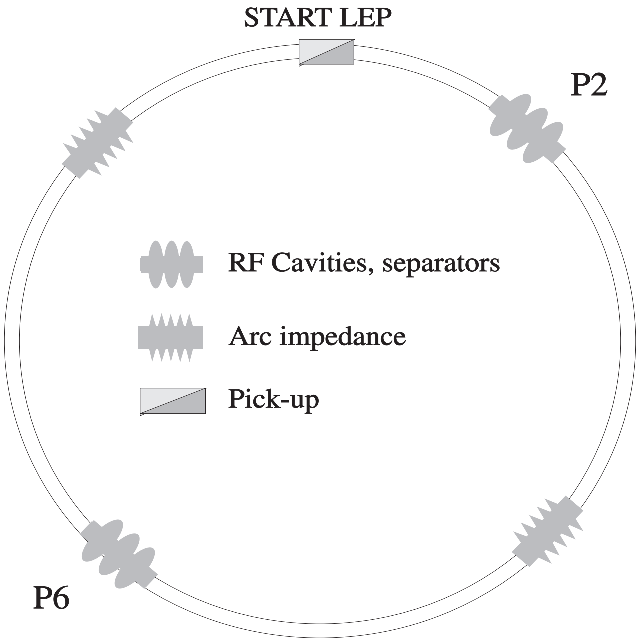

Figure 22: The LEP machine model A

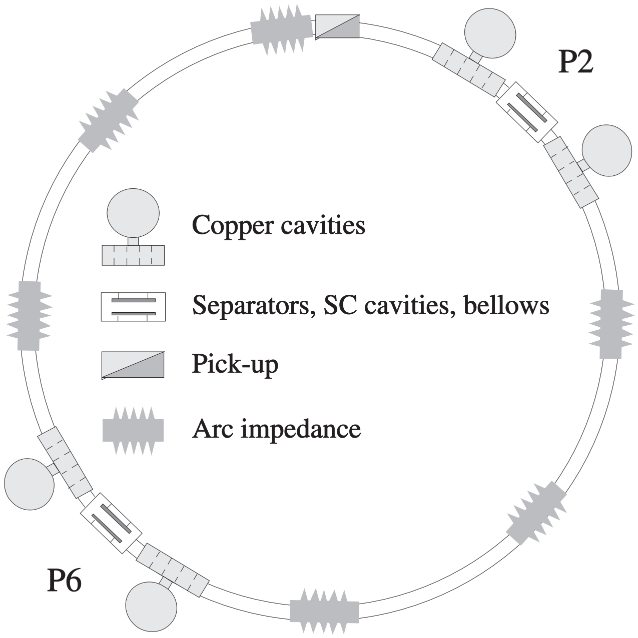

Figure 23: The LEP machine model B

6 Tests and comparisons

6.1 Stability of the simulation results

A correct choice of the number of macroparticles, of the half-length Δ of the basis functions, and of the machine description is an essential complement to the accuracy of the impedance model in order to obtain a good representation of the beam dynamics. For what concerns the first two parameters, the following criteria were formulated in section 2.2:

$$\Delta \in \left[\frac{\sigma}{5}, \frac{\sigma}{2}\right] \tag{21}$$

$$N > F\left(\frac{10\sigma}{\Delta}\right)^2 \tag{22}$$

where σ is the low-current RMS length, and F can vary in the interval $[1, 2]$ depending on the higher current bunch dynamics. For example, a simulation of the bunch lengthening phenomenon, in particular in the presence of turbulence, tends to require a larger N, because modes of higher order are involved in the dynamics. In what follows, the validity of these criteria will be investigated by comparing the simulation results corresponding to different values of N and Δ. The stability of the results with respect to the choice of the machine model will also be discussed.

To perform this test, a typical LEP configuration at injection has been chosen, with Q_s=0.08 and damping wigglers on. In these conditions, the bunch length is known to be around 12mm, and no turbulent lengthening should appear. For the case of the Δ=3mm basis function, σ/Δ is then about 4 ($N_{min} \approx 2000$), while in the case of the Δ=6mm basis function, σ/Δ is about 2 ($N_{min} \approx 500$). Table 6 reports the equilibrium values which have been obtained in the different cases. All jobs were run with 10000 turns, which implies almost 4 damping times, and the average values were taken over the last damping time.

Machine model	Δ mm	Number of particles	Coherent vert. tune	Power loss MeV/turn	RMS length mm	CPU s
A	6	500	0.162	15.8	12.1	284
A	6	1000	0.162	16.0	12.0	568
A	3	2000	0.1615	16.1	12.0	1152
A	3	5000	0.1615	16.0	12.1	3099
B	3	2000	0.162	15.9	12.2	2928

Table 6: Equilibrium values corresponding to different choices of the number of macroparticles, of the length of the basis function, and of the machine model. LEP 90/60 (1993) optics, damping wigglers on at 600A, Q_s=0.08, Q_y=76.21, bunch current I_b=500μA. The power loss is only that relative to the longitudinal wake, while the synchrotron radiation power loss is 7.45 MeV/turn. The radiation damping time is 0.238s ($\approx$ 2700 turns), the average values are taken over the last 3000 turns. The reference wake potentials have been obtained using the ABCI program (see section 4).

The results show a remarkable stability, demonstrating the validity of the criteria (21) and (22). Figures 24, 25 and 26 report three vertical oscillation spectra corresponding to different choices of the simulation parameters, obtained by a Fourier transform of the vertical center-of-charge positions recorded over the last 2000 turns: again, the equivalence of the results is apparent.

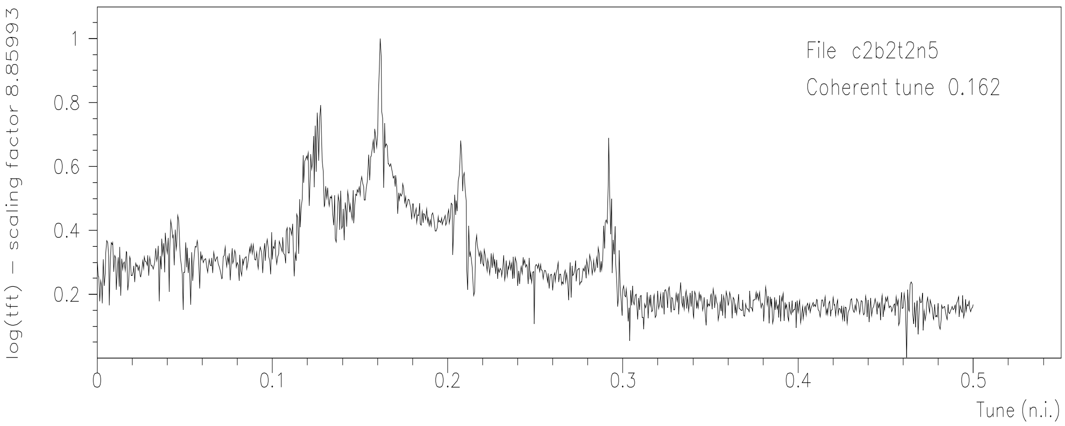

Figure 24: Vertical oscillation modes: Δ=6mm, N=500, machine model A.

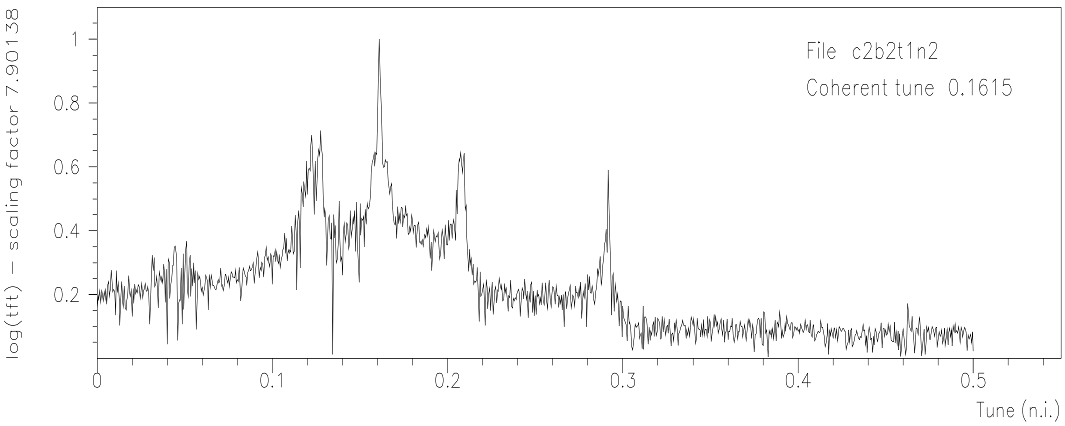

Figure 25: Vertical oscillation modes: Δ=3mm, N=2000, machine model A.

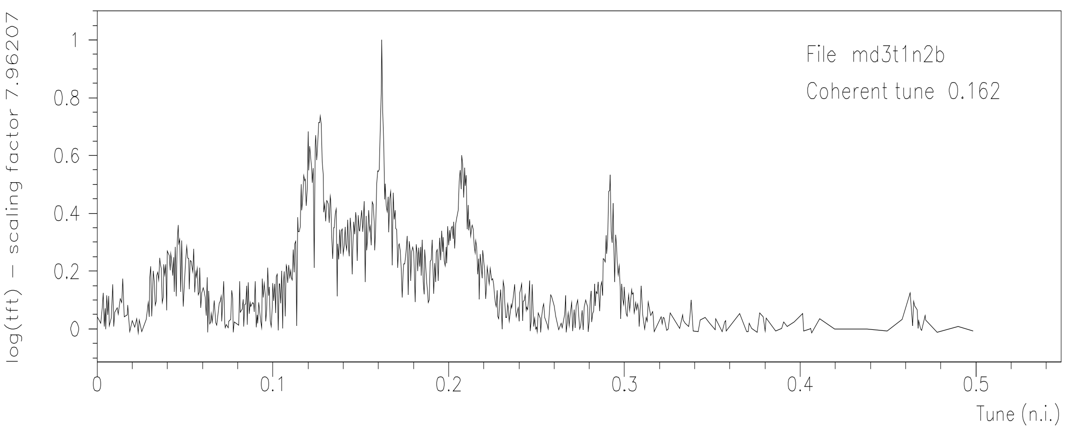

Figure 26: Vertical oscillation modes: Δ=3mm, N=2000, machine model B.

6.2 Comparison with HERSIM

This section is devoted to a comparison between the new wakefield representation in terms of linear intepolating functions and an alternative technique, where the distribution moments are expanded on a basis of Hermite polynomials (see section 2.2). The comparison could be carried out consistently because the two methods were offered as alternative subroutines in the early versions of the TRISIM program.

For this comparison, a very simple model of the LEP accelerator has been used, in which all the RF voltage and all the machine impedance is concentrated in a single point-like element. In order to obtain an equivalent representation of the impedance, the reference wake potentials for both the triangular shaped basis functions and the Hermite polynomials have been computed using a BBR model, namely the one described in section 4 (equations 16); since this model only concerns transverse (vertical) wake potentials, longitudinal effects will not be considered in the comparison.

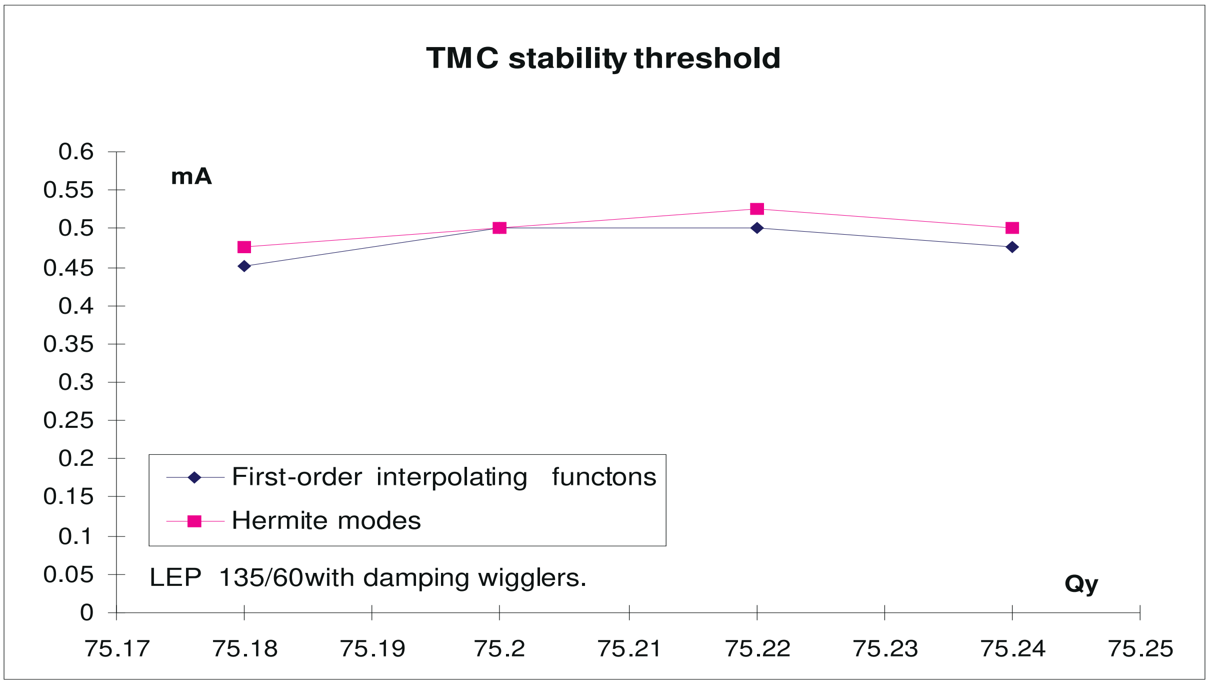

Figure 27: TMC stability threshold vs vertical tune: comparison between the Hermite modes and the first-order interpolating functions. LEP 135/60 (1994) with damping wigglers, Q_s=0.077. N=500 in both cases, Δ=6mm. The reference wake potentials have been computed using the BBR model (16) of LEP impedance.

Figure 27 reports the vertical TMC stability threshold as a function of the vertical tune (the instability threshold has been defined as the current at which the bunch starts to lose particles). The two results are substantially equivalent, although the threshold current obtained with the method based on the Hermite polynomial expansion is slightly higher than that obtained by expanding the distribution moments as sums of linear interpolating functions.

A possible explanation of this phenomenon is the following: the Hermite mode expansion, which is based on the assumpion that the distribution is pseudo-Gaussian, tends to artificially stabilize the bunch, while the expansion in terms of linear interpolating functions, in which no pre-assumption on the distribution shape is present, can more readily follow the evolution towards the instability. This interpretation is confirmed by the results reported in table 7, where it is shown that, for currents below the stabilty threshold, the coherent detuning obtained with the two techniques is identical, so that the differences appear only in the proximity of the stability threshold.

Distribution representation	Number of particles	Coherent vert. tune	CPU (wake)	CPU (tracking)
TRISIM (Δ=20ps)	500	0.181	20	87
Hermite modes	500	0.181	162	91
TRISIM (Δ=20ps)	1000	0.181	31	179
Hermite modes	1000	0.181	224	184

Table 7: Comparison between the Hermite modes and the first-order interpolating functions. LEP 90/60 with damping and polarization wigglers, Q_s=0.083, Q_y=76.23, I_b=500μA. The reference wake potentials have been computed using the BBR model (16) of LEP impedance.

Table 7 also reports the CPU time which has been necessary for the calculation of the wakefield effect with the two techniques. Here the distribution representation based on the linear interpolating functions presents a great advantage with respect to the Hermite modes: the CPU time is in fact reduced by a factor 8 when the new wakefield representation method is used. This does not mean, however, that the total CPU load is reduced of the same factor: the time required for the single-particle tracking along the magnetic arcs is obviously unchanged in both cases: this CPU time, which represents, depending on the number of macroparticles, between half and one third of the total when the Hermite polynomial representation is used, becomes the dominant contribution when the new wakefield representation is used. In these conditions, a significant further reduction of the CPU time could be obtained using a parallel computer: in this case, the bunch could be splitted in as many sub-bunches as the available CPU units, and the single-particle tracking along the arcs could be performed in parallel on each of the sub-bunches. It can be expected that, with 4-5 units available, the total CPU time could be cut to about half of its present value.

7 Applications[8]

7.1 Longitudinal dynamics

Some interesting experimental observations concerning longitudinal collective effects al LEP were reported by D. Brandt et al. [33] at the EPAC 92 Conference in Berlin. The results, which referred to the LEP 90/60 optics, with damping wiggler powered to 400A, can be summarized as follows:

- When looking at the longitudinal spectra during accumulation, the higher harmonics $(f_s)_i$ of the synchrotron frequency progressively appeared, and got surrounded by additional lines, as illustrated in Fig. 29. These additional satellites were identified as radial modes, i.e. modes with the same azimuthal number, but with different radial dependence in the longitudinal phase space. For vanishing beam current, all these modes have the same frequency, but the degeneracy is progressively removed for increasing beam currents. According to theory [34, 35], however, the fundamental modes should evolve into a continuum (infinite number) of radial modes with increasing intensity, while the observations remained of discrete nature; on the other hand, it is clear that only the modes being sufficiently coherent can be actually observed. On top of this, some additional lines could be detected around $(f_s)_2$ after a fine tuning of the analyzer settings.
- For currents above 150μA, a turbulent bunch lengthening was observed; in these conditions, the streak camera showed that the bunch length was steadily oscillating between larger and smaller values: the corresponding minima/maxima, measured as a function of intensity, are reported in Fig. 28.

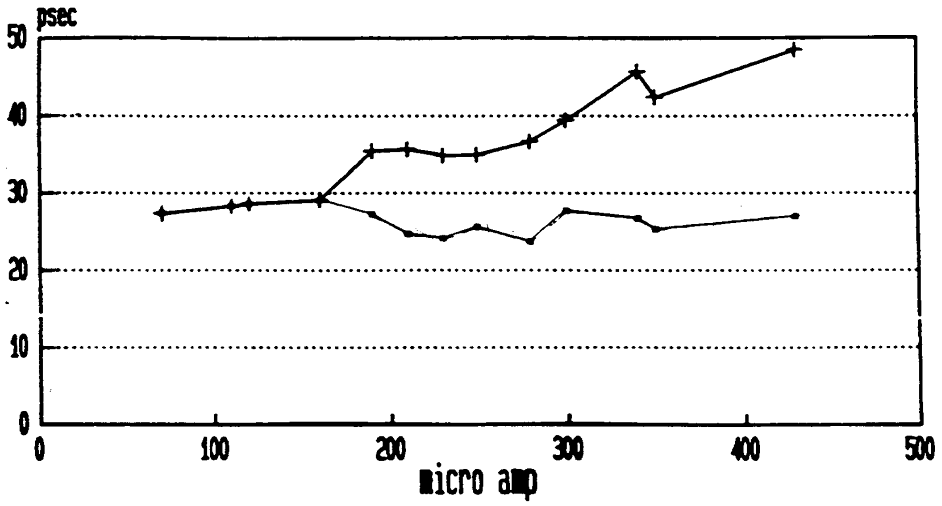

Figure 28: Bunch length as a function of current, as reported in [33]. LEP 90/60 optics, damping wigglers powered to 400A, Q_s=0.085.

[8]The results presented in this section are not meant to provide a comprehensive analysis of the underlying physics: in the context of the present report, they are mainly intended as a demonstration of the capability of the simulation code to correctly represent the physical reality, and as examples of possible applications. A more detailed treatment of these interesting phenomena will be the subject of a dedicated report.

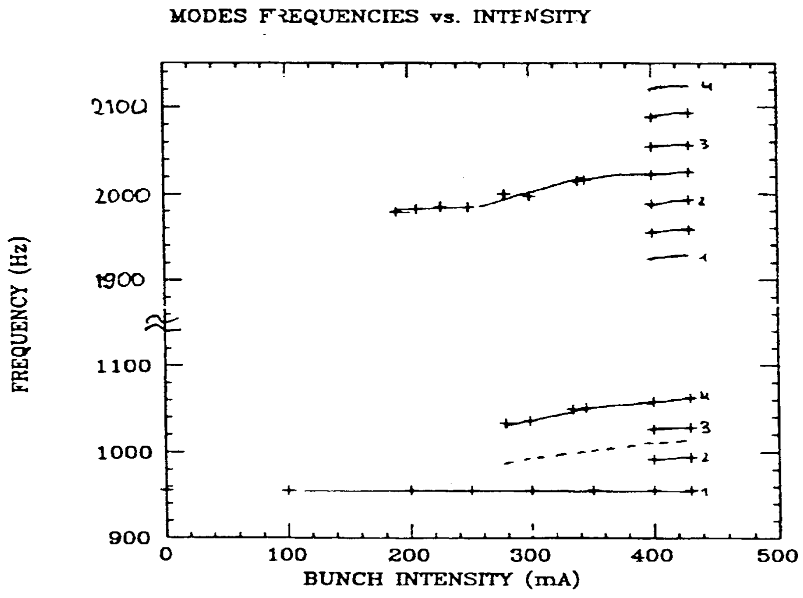

Figure 29: Frequency of the longitudinal modes as a function of intensity, as reported in [33]. LEP 90/60 optics, damping wigglers powered to 400A, Q_s=0.085.

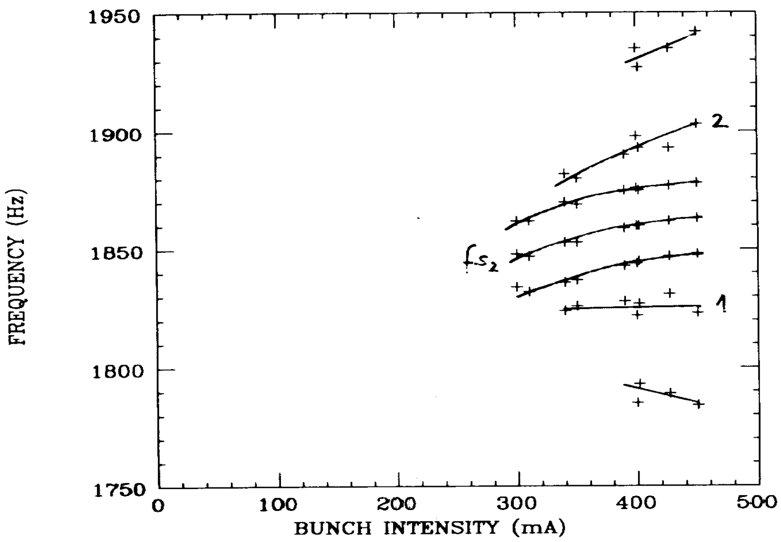

Figure 30: Mode frequencies vs. intensity in the region around $(f_s)_2$. LEP 90/60 optics, damping wigglers powered to 400A, Q_s=0.085. Courtesy D. Brandt.

In order to check the capability of the TRISIM program to reproduce the experimental observation, and possibly to help understanding the physical processes involved, a simulation of the conditions of this machine experiment was carried out, using the LEP machine model A (Fig. 22). Starting from a bunch current equal to zero, an accumulation to 450μA, in steps of 50μA, was simulated. Figure 31 reports the results which were obtained for a bunch current of 450μA: the main machine parameters and simulation conditions are also given, together with the equilibrium values (averaged over 2000 turns), the turn-by-turn plots of the longitudinal center-of-charge position and of the bunch length, and the longitudinal modes of oscillation, obtained by a (2000 turn) Fourier transform of the center-of-charge motion.

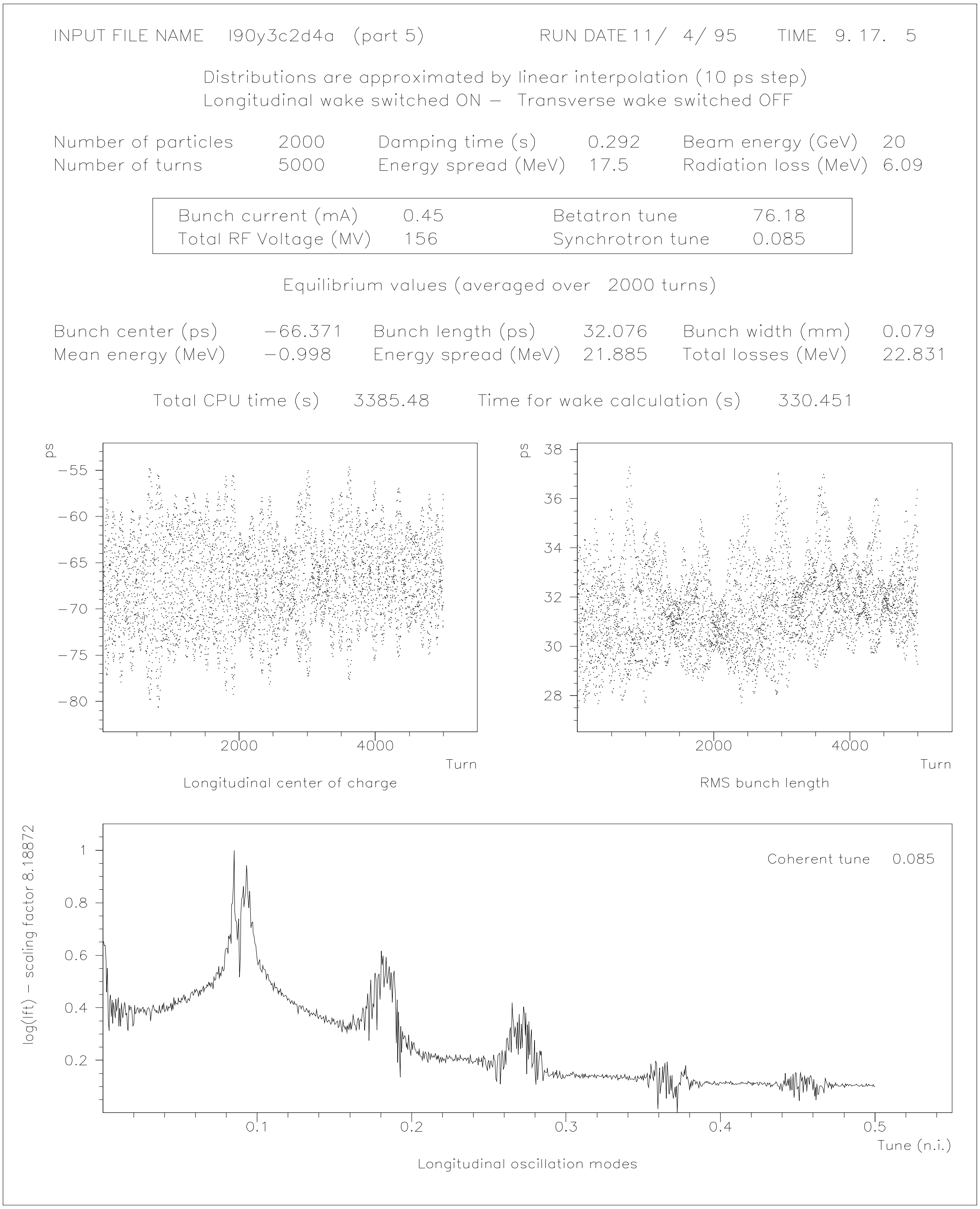

Figure 31: Simulation results for I_b=450μA. LEP 90/60 optics, damping wigglers powered to 400A, Q_s=0.085.

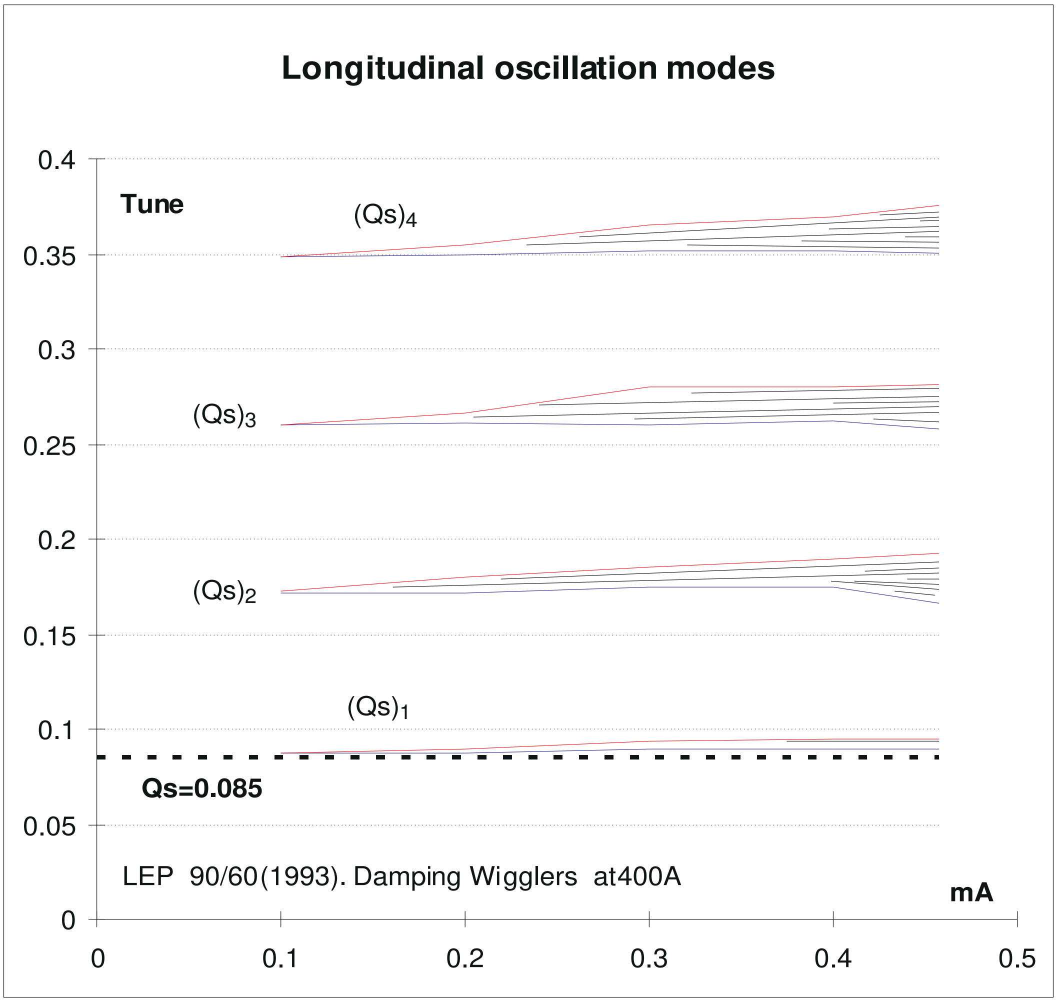

Figure 32: Frequency of the longitudinal modes as a function of intensity, obtained from the TRISIM simulation. LEP 90/60 optics, damping wigglers powered to 400A, Q_s=0.085.

From the longitudinal oscillation mode spectra taken at successive steps in bunch current, figure 32 was obtained: here the tune range corresponding to each cluster of modes appearing around the harmonics of the synchrotron frequency is reported, together with some additional lines which give a qualitative indication of the modes appearing within the cluster. The simulation results exibit most of the features which were observed during the experiment: as the current increases, the number of modes in each cluster grows, the tune range over which the cluster extends gets wider, and, although the general trend is to shift upwards with intensity, the lower end of the cluster is actually moving down, especially at high current (Fig. 30). Another interesting feature which is reproduced by the simulation is that all the $(Q_s)_1$ satellites appear above the synchrotron tune Q_s. On the contrary, an important difference between the simulation results and the experiment is that the modes in each cluster, instead of showing a discrete nature, fill continuously the tune space around each of the Q_s harmonics, as predicted by the theory of radial modes. This residual discrepancy between the model of radial modes and the experimental observations is therefore removed as far as the simulation results are concerned.

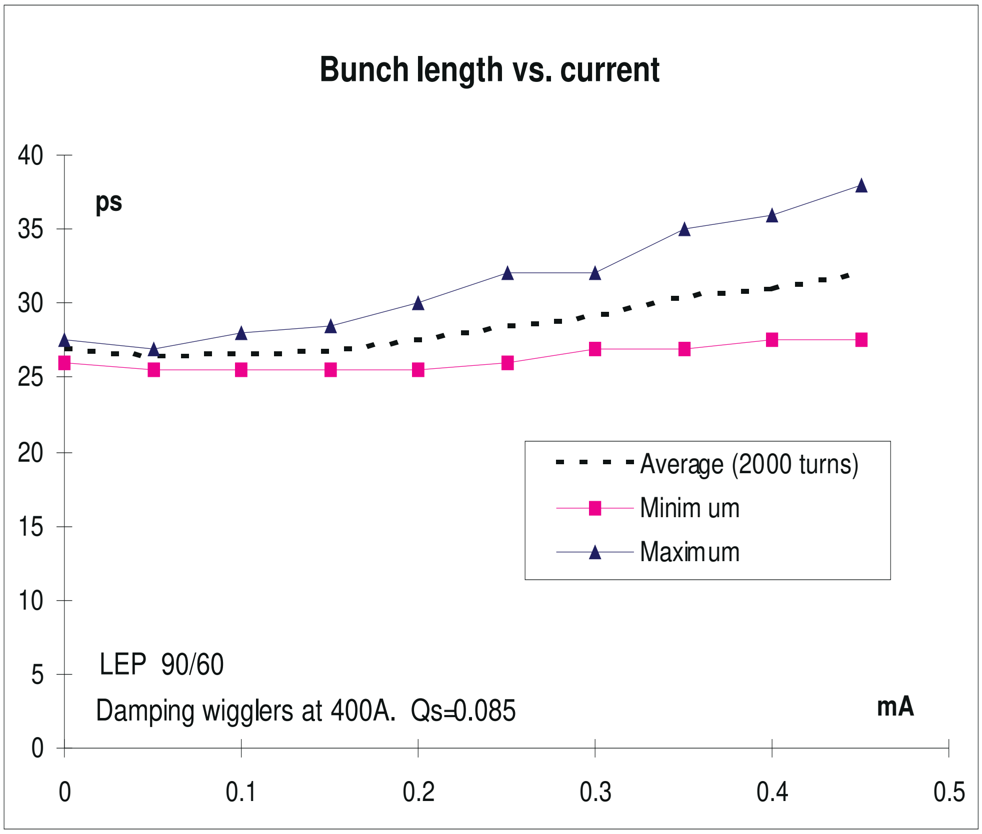

Figure 33: Bunch length vs. intensity, obtained from the TRISIM simulation. LEP 90/60 optics, damping wigglers powered to 400A, Q_s=0.085.

From the plots of the RMS bunch length vs. time (Fig. 31), taken at successive steps in bunch current, figure 33 was obtained. Again, the simulation results are in fair agreement with the experimental observation, with two differences:

- At low (even zero) current, a bunch length oscillation in a range of about 1.5 ps is already present in the simulation results, and it is continuously increasing during accumulation, while the experimenters reported a single bunch length value up to 150μA, where an oscillation in a range of about 8ps suddenly started. However, the low-current bunch length oscillation in the simulated beam is not a collective phenomenon, as it is already present at zero-current; this effect is related to the use of a limited number of macroparticles: in fact, when the simulation is carried out with 10000 particles instead of 2000, the zero-current oscillation range is reduced from 1.5ps to about 0.8ps.
- At high current, the range of the bunch length oscillation of the simulated beam is somewhat smaller than the one observed during the experiment.

In order to further investigate the nature of the longitudinal bunch length oscillations at high current, a dedicated run at 450μA was carried out. First, a 20000 turn tracking was performed in order to get a suitable starting distribution, which was then used as the initial bunch configuration for a shorter 2000 turns run.

The bunch length measurements taken at the pick-up during the first 300 turns are reported in Fig. 34: in each synchrotron period (11-12 turns), two oscillations are performed, the first of smaller amplitude, the second with a larger one. This structure is mantained for about hundred turns, then it is reversed, i.e. the larger amplitude is attained during the first half-period.

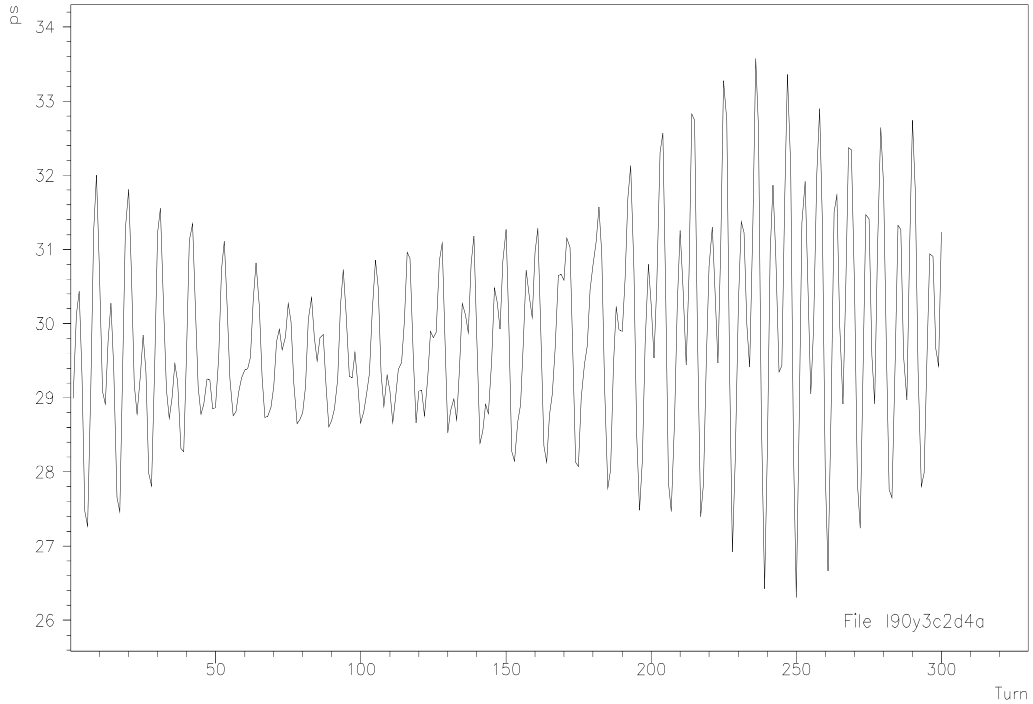

Figure 34: Bunch length vs. turn. LEP 90/60 optics, damping wigglers powered to 400A, I_b=450μA, Q_s=0.085 (simulation).

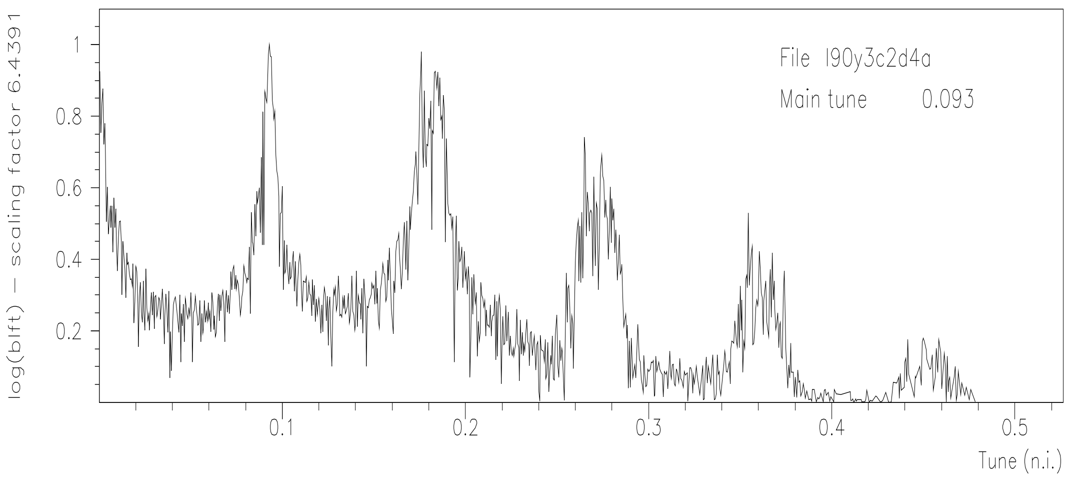

Figure 35: Bunch length oscillation modes. LEP 90/60 optics, damping wigglers powered to 400A, I_b=450μA, Q_s=0.085 (simulation).

Figure 35 reports the frequencies of the bunch length oscillation, obtained by a Fourier transform of the pick-up signal, recorded over 2000 turns. The spectrum is similar to that relative to the center-of-charge motion (Fig. 31), but the peak at the (zero-current) synchrotron tune of 0.085 is no more present. The splitting of the second harmonic of the synchrotron frequency corresponds to the already mentioned modulation of the $2Q_s$ bunch length oscillation.

It is also interesting to show how the bunch shape evolves in the turbulent regime. In figure 37 the longitudinal charge density at successive turns is plotted, from turn 247 to turn 255: this interval has been chosen because here the modulation effect produces a relatively large oscillation amplitude. A detailed plot of the bunch length vs. turn is reported, for comparison, in figure 36. Here it is shown that turn 247 corresponds to one maximum of the large-amplitude oscillation: the bunch shape plot exibits, in these points, a characteristic structure with three peaks, which then shrinks into a single-peak shape corresponding to the minimum bunch length (turn 250). Then an oscillation of smaller amplitude starts, and produces, at its maximum, a double-peak structure (corresponding to the lower maximum in Fig. 36, turn 252), which again decays in a single-peak shape at turn 255.

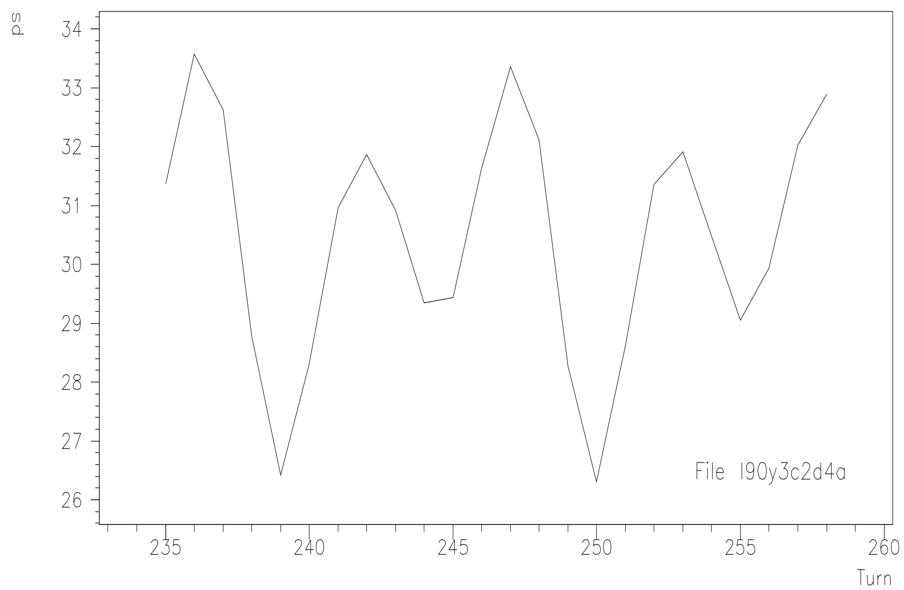

Figure 36: Detailed structure of the bunch length oscillation (for comparison with the longitudinal bunch shape plots of Fig. 37). LEP 90/60 optics, damping wigglers powered to 400A, I_b=450μA, Q_s=0.085.

It was mentioned in section 3 that, despite their small longitudinal loss factors, the tapers and the bellows can have an important role in the onset of longitudinal turbulence, because their rapidly oscillating wake potential (Fig. 16) provides a high frequency component in the potential well, which provokes higher order (quadrupole, sextupole...) oscillations of the bunch shape. To show this, the simulation of the machine experiment has been repeated using a new impedance model, in which all the contributions from tapers and bellows have been removed. With the new impedance model, at 450μA, no longitudinal turbulence appears: the average bunch length is now 21.7 ps, to be compared with a theoretical zero-current value of 27 ps, and the amplitude of the oscillation around the average value is about 1 ps when 2000 macroparticles are used (as it was already mentioned, this oscillation is an incoherent effect linked to the use of

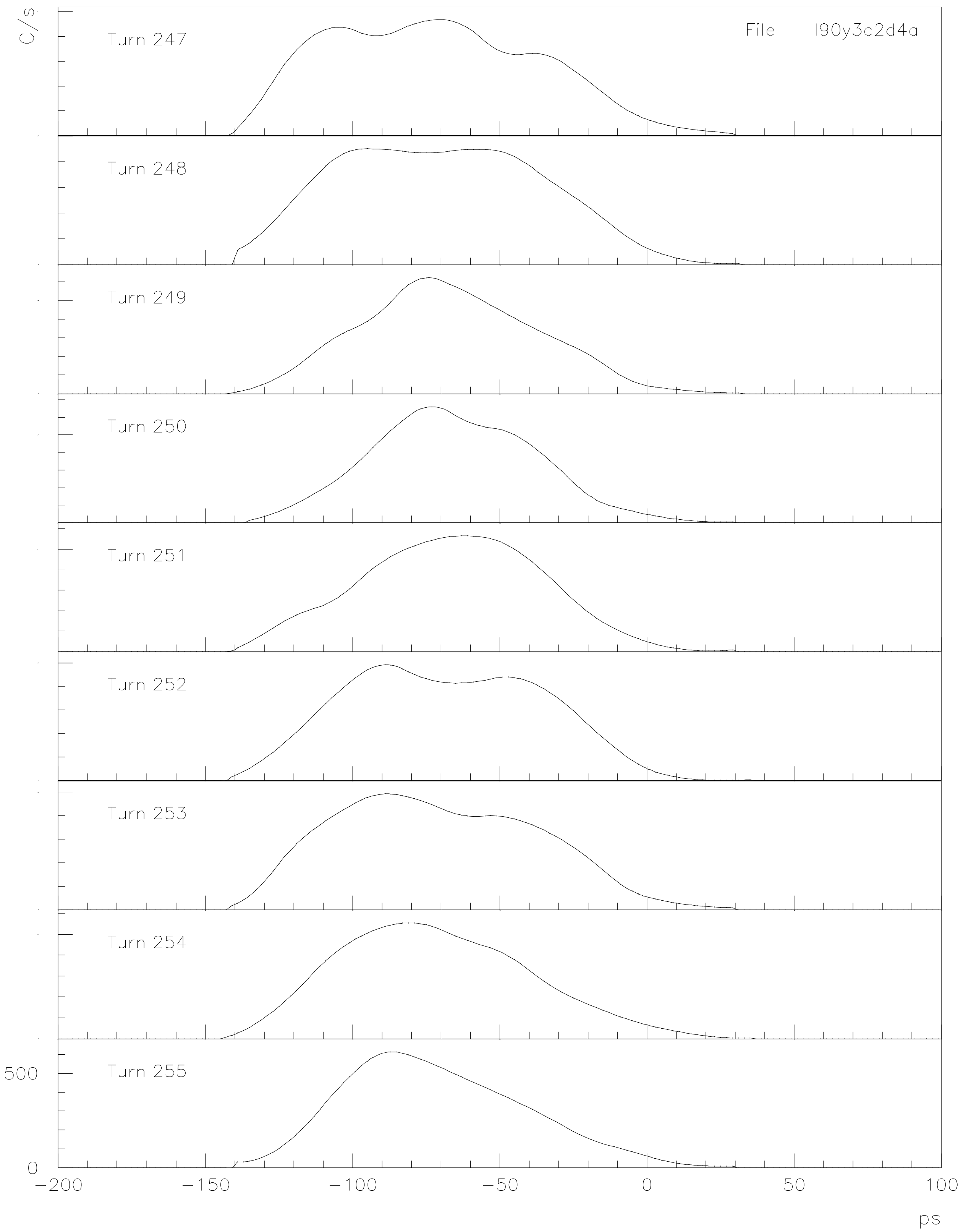

Figure 37: Bunch shape vs. turn. LEP 90/60 optics, damping wigglers powered to 400A, I_b=450μA, Q_s=0.085.

a limited number of macroparticles). Figure 38, in which the bunch shape vs. turn is reported, shows that the distribution remains approximately Gaussian, with the main peak performing a small dipole ocillation around the center of the distribution, while no higher modes of oscillation are present.

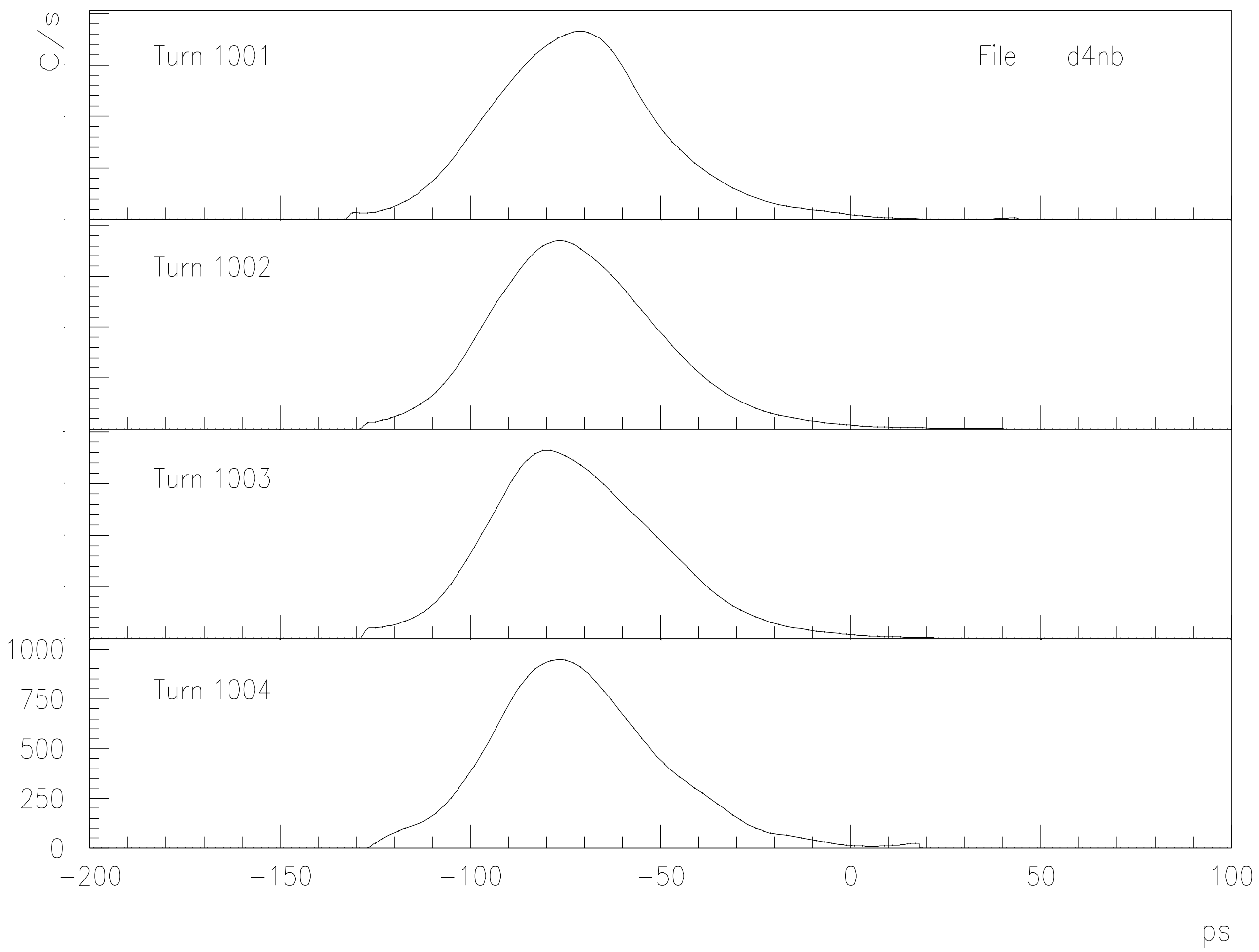

Figure 38: Bunch shape vs. turn: the conditions are the same of Fig. 37, but the contributions of bellows and tapers have been removed from the impedance model.

Another interesting effect related to the longitudinal impedance of the bellows is the negative shift with current of the $(Q_s)_2$ mode, which has been observed, for short bunches, in a recent machine experiment at LEP [36]. This effect was considered quite strange, because the standard model predicts capacitive coupling for short bunches and inductive coupling for long bunches, while at LEP an opposite behaviour is observed.

The simulation of the conditions of the experiment (no wigglers, Q_s=0.08) confirms the negative shift of the main peak in the $(Q_s)_2$ cluster of modes with respect to $2Q_s$, as shown in figure 39 for a bunch current of 50μA; it should be noted, however, that the cluster extends on both sides of $2Q_s$. It should also be noted that the simulation predicts, in these conditions, a bunch length of 3.5 mm, while a bunch length of 6.3 mm was measured during the experiment: this difference is quite important, because when a bunch length around 6 mm is simulated (for example by exciting the wigglers) a capacitive coupling is observed.

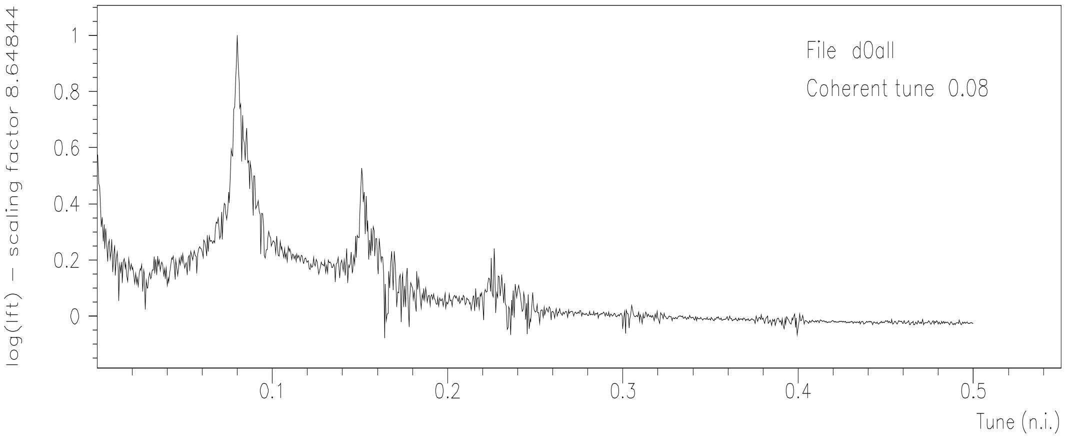

Figure 39: Longitudinal oscillation modes, when all the machine impedance is included in the model. LEP 90/60, no wigglers, Q_s=0.08.

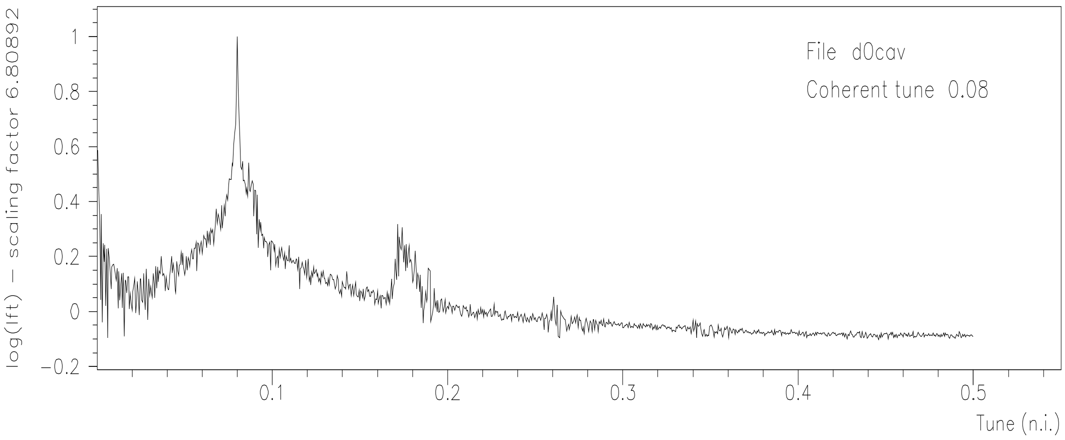

Figure 40: Longitudinal oscillation modes, when only the cavity impedance is included in the model. LEP 90/60, no wigglers, Q_s=0.08.

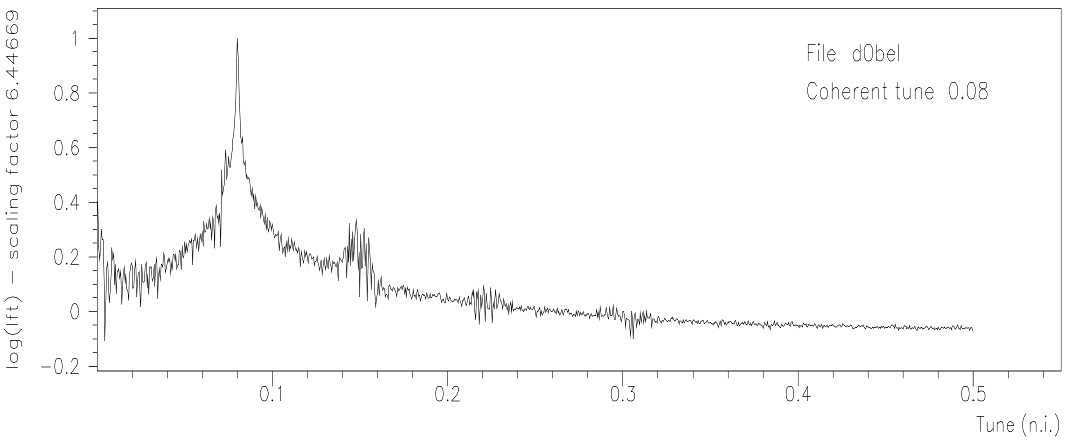

Figure 41: Longitudinal oscillation modes, when only the bellows impedance is included in the model. LEP 90/60, no wigglers, Q_s=0.08.

In order to investigate the origin of the inductive coupling for short bunches, the simulation of the conditions of the experiment has been repeated using two modified impedance models, in which either the contributions of the cavities or that of the bellows has been removed. The results are reported in figures 40 and 41, which show that when only the cavities are present, the $(Q_s)_2$ cluster is completely shifted to the right of $2Q_s$, while the opposite is true when only the bellows impedance is included in the model.

The unusual behaviour of the $(Q_s)_2$ shift observed at LEP can then be explained by modelling the longitudinal impedance as the superposition of two LRC resonators with different resonant frequencies. Each single resonator is inductive at low frequencies (i.e. long bunches) and capacitive at high frequencies (i.e. short bunches), but when the two resonators are superimposed the situation becomes more complex: while the standard model still holds in the lower ($|\omega| < \omega_{r1}$) and in the upper ($|\omega| > \omega_{r2}$) parts of the spectrum, in the intermediate region different situations may occurr, depending on the relative amplitude of the two bumps. At LEP, assuming a resonant frequency $\omega_{r1} \approx$ 1-2 GHz for the cavities, and a resonant frequency $\omega_{r2} \approx$ 20-50 GHz for the bellows, both the "long" (10mm) and the "short" (3mm) bunches sit in the intermediate region of the spectrum. The simulation results show that the positive bump of the cavities dominates in the lower part of this region (1-10 GHz, "long" bunches), while the negative bump of the bellows is dominant in the upper part (10-20 GHz, "short" bunches).

7.2 Transverse dynamics

The transverse mode coupling instability is known to be the main intensity limitation of the single bunch current of LEP at injection. One possible strategy in order to circumvent the present limitation is to accumulate with a higher synchrotron tune Q_s. The advantage of an increase of the synchrotron tune can be easily explained, as it increases the natural (zero-current) frequency separation between the rigid dipole vertical oscillation mode m=0 and the head-tail mode m=-1, the coupling of which is responsible for the onset of the TMC instability. Equation (14) also indicates that the stability threshold increases with Q_s; however, it should be noted that increasing Q_s shortens the bunch length which, in turn, increases the loss factor, as indicated by the curves in fig. 13. Moreover, the high-Q_s operation may result in other undesirable effects, like the onset of longitudinal turbulence or the appearence of new synchro-betatron resonances. The possibility of obtaining a real gain then depends on the combination of all these effects.

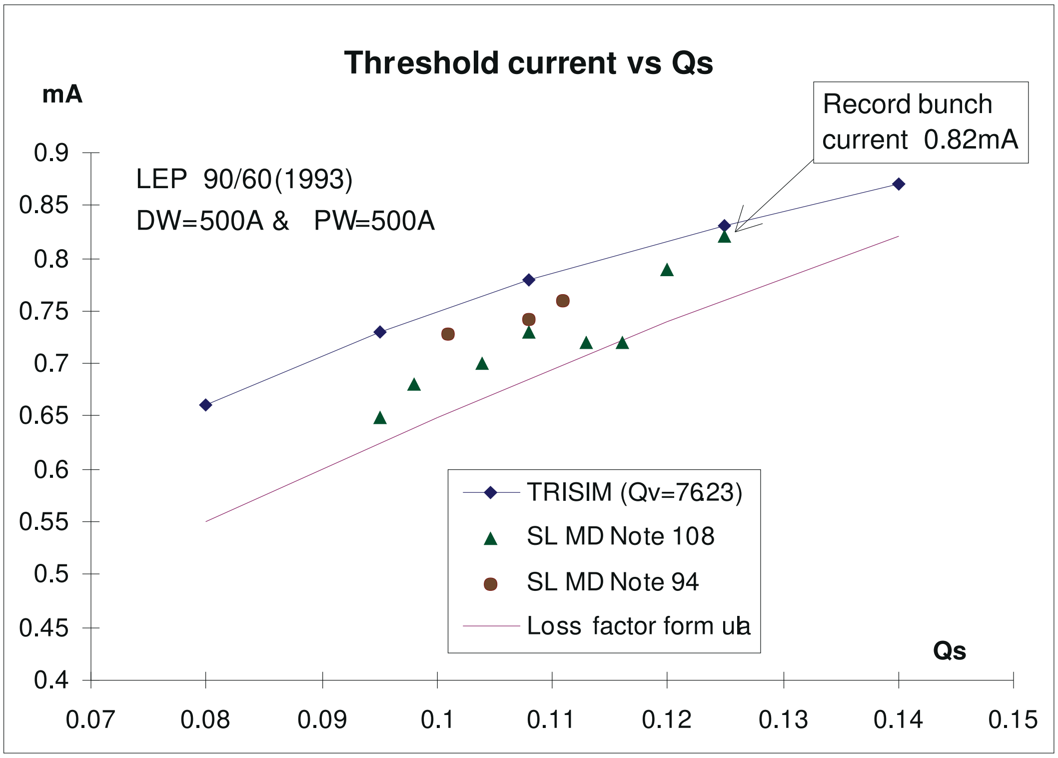

Figure 42: TMC threshold current as a function of Q_s. The curve indicated as "loss factor formula" has been obtained from equation 14, using the loss factor dependence on bunch length reported in Fig. 13. For each value of Q_s and Q_v, the current threshold calculated with TRISIM has been obtained by simulating an accumulation process in steps of 20 μA, and checking at which current the bunch starts losing particles.

The high-Q_s operation has been both tested experimentally [37, 38] and simulated with TRISIM. The results are presented in Fig. 42: the simulations are in very good agreement with the measurements. As can be seen, rather interesting gains can be achieved in the nominal operating conditions: in fact, the highest point in the curve indicated as "SL MD Note 108" corresponds to the record bunch current ever obtained at LEP. However, it was found that when the synchrotron tune Q_s is increased, the dependence of the threshold current on the betatron tune becomes stronger. This reduction of the optimal tune space can be related to coherent synchro-betatron resonances driven by the onset of turbulence in the longitudinal plane [36]. Other mechanisms could also be involved, like the presence of instability stop bands due to coupling between low-order and high-order (reflected) modes [39, 40]: such coupling can be better observed for relatively short bunches, when the higher order modes more easily appear on the spectrum, as shown by the simulation results in figure 43, but it is also experienced by longer bunches; the presence of clusters of radial modes can further reduce the tune space available. For all these reasons, more studies concerning operation at high-Q_s are needed, in order to check up to what limits the scheme can be applied.

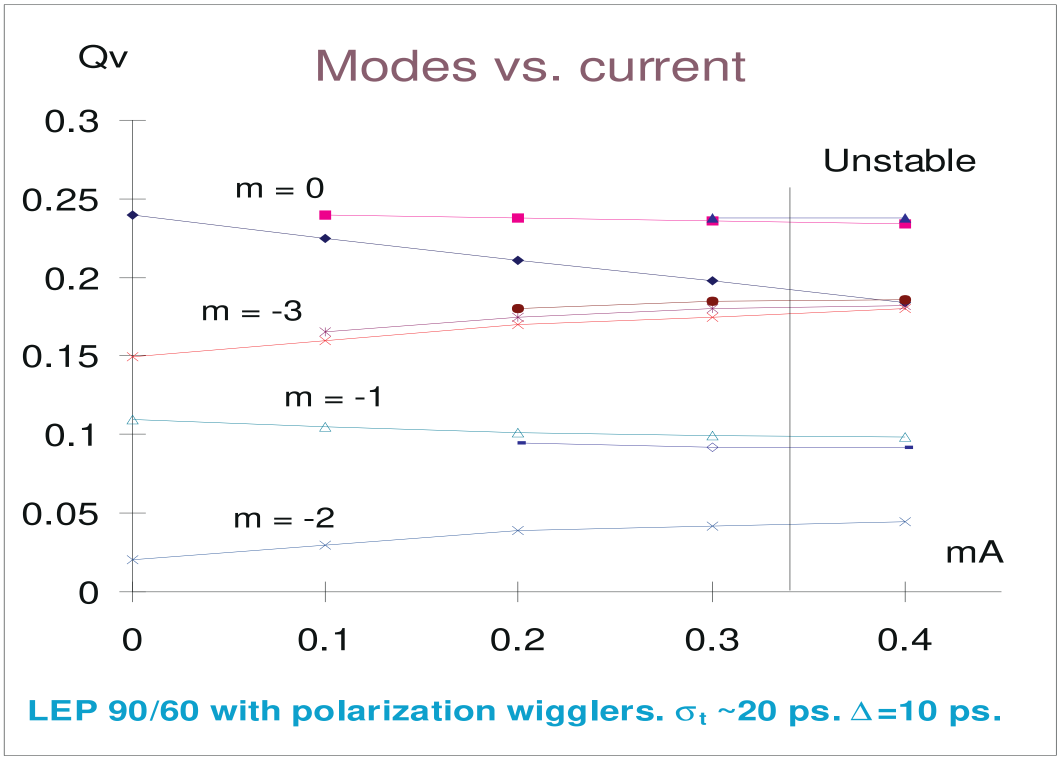

Figure 43: Coupling between low-order and high-order (reflected) modes (simulation).

8 Conclusions

A new method for modelling wakefield effects in multi-particle tracking progams has been presented. This method is based on an expansion of the distribution of the charge density, and of its transverse moment, on a basis of linear interpolating functions: as compared with other possible choices of the basis functions, like Hermite polynomials or (binned) point charges, the use of linear interpolating functions allows a better representation of the distribution; at the same time, a strong reduction of the CPU time and of the memory requirements could be achieved: the reason is that the use of linear functions as basis functions allows a full exploitation of the linearity of Maxwell equations in the calculation of the wake potential; on top of this, the resulting procedure is very well suited to the implementation on a digital computer.

The simulation program TRISIM is based on the new wakefield representation method. Using refined estimates for the impedances in LEP, it was possible to get quite good agreement with measurements in the simulation of both longitudinal and transverse collective effects. Predictions on the future operation of the machine, and in particular for LEP2, can thus be based confidently on this code. The program has also been used to study a new reactive feedback system using additional passive oscillators [41], and to evaluate its effectiveness and sensitivity to errors [42]. In addition, the simulation code has proved to be a valuable tool to study and explain observations made during machine experiments, such as synchro-betatron resonances and mode splitting at higher currents.

Acknowledgements

The author would like to thank very cordially Bruno Zotter and Daniel Brandt for their help and for many fruitful and enlightening discussions. He also would like to thank all the members of the AP group, in particular Jacques Gareyte, for their kind hospitality.

References

[1] G. Sabbi, *"TRISIM User's Guide"*, CERN SL/94-73 (AP), August 1994.

[2] T.S. Wang, *"HERSIM2"*, CERN Div. Report SL/90-08, 1990.

[3] V. Nys, *"Computer simulation of a transverse single bunch instability"*, CERN Div. Report LEP-TH/87-35, 1987.

[4] D. Brandt, *"SIMTRAC - A simulation program for tracking longitudinal and transverse single-bunch effects"*, CERN LEP-Note 512, 1984.

[5] B. Zotter, *"Improved Equations of motion for multi-particle simulation"*, CERN SL Note, 1993.

[6] A. Chao, *"Physics of collective beam instabilities in high energy accelerators"*, John Wiley & Sons, 1993.

[7] G. Sabbi, Ph.D. Thesis, University of Genoa, 1994.

[8] E. Keil, *"Diffraction radiation of charged rings moving in a corrugated cylindrical pipe"*, Nucl. Instrum. Meth., 100, 419 (1972).

[9] K. Bane, P. Wilson, *"Longitudinal and transverse wake potentials at SLAC"*, Proc. of the 11th Int. Conf, on High Energy Accelerators, CERN, 1980.

[10] D. Brandt, B. Zotter, *"Calculation of the wakefield with the optical resonator model"*, CERN-ISR/TH/82-13, 1982.

[11] D. Brandt, *"Simulation of longitudinal single-bunch effects in LEP"*, CERN/ISR-TH/82-09, May 1982.

[12] K. L. Bane, *Wakefield effects in a linear collider"*, AIP Conf. Proc. 153 (AIP New York, 1987), pp. 971-1012.

[13] T.S. Wang, B. Zotter, *" A new wake potential calculation method using orthogonal polynomials"*, IEEE Particle Accelerator Conference, S. Francisco, 1991.

[14] B. Zotter, *"The equivalent broad-band impedance in LEP"*, CERN LEP-TH/87-34, 1987.

[15] D. Brandt, K. Cornelis, T. Fieguth, A. Hofmann, J. Jowett, S. Myers, E. Peshardt, M. Placidi, L. Rivkin, B. Zotter, *"Intensity limitations and the impedance of LEP"*, EPAC 90 Conference, Nice, June 1990.

[16] Y. Chin, *"The wake field acceleration using a cavity of elliptical cross section. Part1: WELL"*, KEK Report 83-19, November 1983.

[17] Y. Chin, *"Transverse impedance in elliptic vacuum chamber components and beam separators in LEP"*, LEP Theory Note 33, December 1984.

[18] R. Klatt et al., *"MAFIA - A three-dimensional electromagnetic CAD system for magnetic, RF structures, and transient wake field calculations"*, SLAC report 303 (1986).

[19] Y.H. Chin, *"ABCI User's Guide"*, LBL Report 33091, 1992.

[20] Guangxiao Li, private communication.

[21] B. Zotter, *"Collective Effects"*, 3rd workshop on LEP performance, Chamonix, January 1993.

[22] A. Taflove, *" Rewiew of the formulation and applications of the finite-difference time-domain method for numerical modeling of electromagnetic wave interaction with arbitrary structures"*, Wave Motion, vol. 10, no. 6, pp. 547-582, 1988.

[23] T. Weiland, *"Transverse beam cavity interaction"*, DESY-82-015, March 1982.

[24] T. Jurgens, F. Harfoush, *"Conformal FDTD modelling of 3D wake fields"*, IEEE Particle Accelerator Conference, S. Francisco, 1991.

[25] G. Aharonian, R. Meller, R. H. Siemann, *"Transverse wakefield calculations"*, Nuclear Instruments and Methods 212 (1983), pp. 23-35.

[26] O. Napoly, Y. Chin, B. Zotter, *"A generalized method for calculating wake potentials"*, Nucl. Instrum. Methods, A334, 255 (1993).

[27] B. Zotter, *"Comparison of theory and experiment on beam impedances: the case of LEP"*, Proceedings of the 3rd European Particle Accelerator Conference (EPAC 92), Berlin, March 1992, pp. 273-276.

[28] B. Zotter, LEP Note 363 (1982).

[29] A. Khursheed, *"The use of finite elements to compute transient electromagnetic fields in accelerating structures"*, CERN LEP-RF/87-40.

[30] O. C. Zienkiewicz, *"The finite element method"*, 3rd ed. New York, Mc Graw-Hill, 1977.

[31] G. Le Meur, F Touze, *"PRIAM/ANTIGONE: a 2D/3D package for accelerator design"*, EPAC 94 Conference, London, June 1994.

[32] B. Schorr, *"Spline estimation of distributions and density functions"*, CERN DD/75/13, 1975.

[33] D. Brandt, K. Cornelis, A. Hofmann, *"Experimental observations of instabilities in the frequency domain at LEP"*, Proceedings of the 3rd European Particle Accelerator Conference (EPAC 92), Berlin, March 1992, pp. 345-347.

[34] F. Sacherer, *Bunch lengthening and the microwave instability*, CERN/PS/BR 77-5 and 77-6 (1977).

[35] K. Oide, K. Yokoya, KEK-90-10 (1990).

[36] K. Cornelis, *"How can we get 1mA per bunch at 20 GeV"*, Proceedings of the fifth workshop on LEP performance, Chamonix, January 13-18, 1995.

[37] D. Brandt, H. Burkhardt, P. Collier, E. Ciapala, K. Cornelis, V. Danilov, G. Geschonke, K. Hanke, A. Hofmann, J. Jowett, E. Perevedentsev, E. Rossa, F. Ruggiero, H. Schmickler, I. Uythoven, B. Zotter, *"Bunch current limit with high Q_s and octupoles"*, SL-MD Note 94, August 1993.

[38] D. Brandt, K. Cornelis, A. Hofmann, M. Lamont, E. Peshardt, B. Zotter, *"Maximum intensity with two beams and high Q_s*, SL-MD Note 108, November 1993.

[39] F. Ruggiero, *"Theoretical aspects of some collective instabilities in high-energy particle storage rings"*, CERN 86-06, Lep Main Ring Division, August 8, 1986.

[40] G. Besnier, D. Brandt, B. Zotter, *"The transverse mode coupling instability in large storage rings"*, Particle Accelerators, Vol. 17, pp. 51-77 (1985).

[41] V. Danilov and E. Perevedentsev, *"Feedback system for elimination of the transverse mode coupling instability"*, CERN Div. Report SL/93-38, 1993.

[42] G. Sabbi, *"Simulation of transverse feedback systems at LEP"*, Cern Report, in preparation.